The Cryosphere, 9, 2119–2134, 2015
www.the-cryosphere.net/9/2119/2015/
doi:10.5194/tc-9-2119-2015

The Cryosphere Open Access EGU

A prognostic model of the sea-ice floe size and thickness distribution

C. Horvat and E. Tziperman

School of Engineering and Applied Sciences and Department of Earth and Planetary Sciences, Harvard University, Cambridge, MA, USA

Correspondence to: C. Horvat (horvat@fas.harvard.edu)

Received: 30 April 2015 – Published in The Cryosphere Discuss.: 28 May 2015
Revised: 14 October 2015 – Accepted: 29 October 2015 – Published: 18 November 2015

Abstract. Sea ice exhibits considerable seasonal and longer-term variations in extent, concentration, thickness, and age, and is characterized by a complex and continuously changing distribution of floe sizes and thicknesses, particularly in the marginal ice zone (MIZ). Models of sea ice used in current climate models keep track of its concentration and of the distribution of ice thicknesses, but do not account for the floe size distribution and its potential effects on air–sea exchange and sea-ice evolution. Accurately capturing sea-ice variability in climate models may require a better understanding and representation of the distribution of floe sizes and thicknesses. We develop and demonstrate a model for the evolution of the joint sea-ice floe size and thickness distribution that depends on atmospheric and oceanic forcing fields. The model accounts for effects due to multiple processes that are active in the MIZ and seasonal ice zones: freezing and melting along the lateral side and base of floes, mechanical interactions due to floe collisions (ridging and rafting), and sea-ice fracture due to wave propagation in the MIZ. The model is then examined and demonstrated in a series of idealized test cases.

1 Introduction

Sea ice is a major component of the climate system, covering about 12 % of the ocean surface. It drives the ice-albedo feedback, a potential source of climate instability and polar amplification, and it affects deep water formation and air–sea fluxes of heat, fresh water, and momentum between the atmosphere and ocean. Its presence also provides a platform for high-latitude ecosystems and determines polar shipping routes. Additionally, sea ice is well-correlated with patterns of atmospheric variability such as the North Atlantic Oscillation (Strong et al., 2009), the Antarctic Oscillation (Wu and Zhang, 2011), and the Madden–Julian Oscillation (Henderson et al., 2014). Over the past few decades, Arctic sea ice has become thinner, less extensive, and more seasonal (Cavalieri and Parkinson, 2012). Regions that were once covered by ice year-round now are ice-free in the summer (Stroeve et al., 2012), and the Arctic marginal ice zone, defined as either the region of the ocean over which waves lead to the fracture of ice (e.g. Williams et al., 2013b), or as the area of ice with concentration between 15 and 80 %, which has been widening during the summer season (Strong and Rigor, 2013). High-latitude storms are capable of breaking thinning pack ice into smaller floes, changing ocean circulation and air–sea exchange (Asplin et al., 2012; Zhang et al., 2013; Kohout et al., 2015), with evidence suggesting that these storms will become more prevalent in the future (Vavrus et al., 2012).

Sea-ice cover is heterogeneous, composed of a distribution of floes of different areas and thicknesses. Floes can vary dramatically in size, ranging from newly formed frazil crystals millimeters in size, to pack ice in the Canadian Arctic with floes up to 10 m thick in places and hundreds of kilometers wide. The most dramatic intra-annual variability in sea-ice cover is found in the MIZ, and in seasonal ice zones, regions which range from being ice-covered to ice-free over the year. As summer sea-ice cover becomes thinner and more fractured, these regions will become larger, and the distribution of these floes and their size, shape, and properties may change. Events that generate surface waves, such as a fortuitously observed Arctic cyclone in 2011, the so-called “Great Arctic Cyclone” of 2012, and an energetic wave event observed in the Barents Sea, can lead to the fracturing of floes (Asplin et al., 2012; Zhang et al., 2013; Collins et al., 2015). The fractured sea-ice cover has increased floe perimeter, which may lead to enhanced melting and a more

rapid reduction in sea-ice area compared to an unfractured sea-ice cover. Steele (1992) indeed demonstrated an increasing sensitivity of the ice cover to lateral melting with decreasing floe size, finding that below 30 m, lateral melting was critically important. Smaller floe sizes may additionally lead to changes in the mechanical response of the sea-ice cover to forcing from the ocean and atmosphere, as floe size is a parameter in collisional models of ice rheology (Shen et al., 1986, 1987; Feltham, 2005, 2008). As sea ice attenuates wave energy, the diminished ice fraction may lead to further surface wave propagation into the ice field, enhancing fracturing farther from the sea-ice edge, and leading to further sea-ice area loss in a positive feedback loop (Asplin et al., 2014). Floe sizes can also affect the surface drag coefficient and therefore air–sea fluxes (Birnbaum and Lüpkes, 2002). Along floe edges, ocean eddies may be generated due to the gradient in surface heat and stress boundary conditions between ice edge and open water (Niebauer, 1982; Johannessen et al., 1987). These eddies may more rapidly mix air–sea heat flux absorbed by open water to underneath sea-ice floes when floe sizes are comparable to the eddy length scale, but not when floe sizes are much larger. This in turn may have consequences for ice melt rates and ocean circulation (Horvat and Tziperman, 2014).

Given that it is not computationally practical to simulate all individual floes, properties of the ice cover can instead be described using statistical distributions. This approach was pioneered by Thorndike et al. (1975), who developed a framework for simulating the ice thickness distribution (ITD), $g(h)$, defined such that $g(h)dh$ is the fractional area of the sea surface covered by ice with thickness between h and $h+dh$. The Thorndike model evolves the prognostic equation

$$\frac{\partial g(h)}{\partial t} = -\nabla \cdot (g\,\boldsymbol{u}) - \frac{\partial}{\partial h}(g(h)G_{\mathrm{h}}) + \psi, \tag{1}$$

where $\boldsymbol{u}$ is the horizontal ice velocity, G_{h} is the rate of change of ice thickness due to melting and freezing (thermodynamics), and ψ, the "redistribution function", describes the creation of ice of thickness h by mechanical combination of ice of different thicknesses. Measurements of ice thickness are made possible by a variety of remote sensing techniques such as submarine sonar, fixed moorings, helicopter borne electromagnetic induction, and satellite measurements (Bourke and Garrett, 1987; Yu and Rothrock, 1996; Renner and Gerland, 2014), which may be used to test model skill. Variants of the Thorndike model have been implemented in several general circulation models (GCMs, Bitz, 2008; Hunke et al., 2013), and have been used to understand sea-ice behavior and predictability (Bitz et al., 2001; Chevallier and Salas-Mélia, 2012).

Modern approaches to modeling sea ice in GCMs, such as the community ice model (Hunke et al., 2013), generally approximate ice cover as a non-Newtonian fluid with vertically layered thermodynamics, and simple thickness distribution (Thorndike et al., 1975; Semtner, 1976; Hibler, 1979). This approximation may not suffice, because it does not account for the distribution of floe sizes and therefore for the above-mentioned related effects.

Table 1. Variables appearing in several components of the FSTD model.

Variable	Description	Section
$g(h)$	Ice thickness distribution (ITD)	1
$\boldsymbol{u}$	Ice velocity vector	1
ψ	Ice thickness redistribution function	1
$n(r)$	Ice floe size distribution (FSD)	1
$\boldsymbol{r} = (r, h)$	Floe size and thickness	1
$f(\boldsymbol{r})$	Joint floe size and thickness distribution (FSTD)	1
ϕ	Open water fraction	2.1
c	Ice concentration	2.1
$N(\boldsymbol{r})$	Floe number distribution	2.1
$C(\boldsymbol{r})$	Cumulative floe number distribution	2.1

We aim to describe the subgrid-scale variability of the sea-ice cover by extending the ice thickness distribution to a joint distribution that includes both ice thickness and floe size. Rothrock and Thorndike (1984) were among the first to describe the distribution of lateral floe sizes, defining the floe size distribution (FSD) $n(r)\,dr$ as the fractional area of the sea surface covered by floes with lateral size between r and $r+dr$. The size of a floe with area a is represented by its effective radius, $r = \sqrt{a/\pi}$, which represents floes as cylinders of radius r. Modeling of the lateral floe size distribution is hampered by the difficulty of measurement, as floe sizes vary over many orders of magnitude. Even with sufficient imagery, algorithms that identify and measure floes must overcome many obstacles, such as submerged floes, melt ponds, and clouds. In spite of these challenges, many observations of the floe size distribution have been made, often using helicopter or ship-board cameras, notably in the Alaskan and Russian Arctic (Holt and Martin, 2001), Sea of Okhotsk (Toyota and Enomoto, 2002; Toyota et al., 2006), Prydz Bay (Lu et al., 2008), and Weddell Sea (Herman, 2010; Toyota et al., 2011). These studies have focused on deriving and fitting scaling relationships measured distributions, leading to power-law (Toyota et al., 2006), Pareto (Herman, 2010), or joined power-law (Toyota et al., 2011) distributions of floe sizes. The temporal evolution of the floe size distribution has been examined in a small number of observational studies (Holt and Martin, 2001; Steer et al., 2008; Perovich and Jones, 2014), that analyzed the change in the floe size distribution over several weeks or seasonally, but these observations, particularly in the marginal ice zone, are limited.

Herman (2010) modeled the FSD as a generalized Lotka–Volterra system, which exhibits a Pareto distribution of floe sizes as a solution, and suggested that this distribution might fit observed FSDs. Toyota et al. (2011) showed that observed

FSDs in the Weddell Sea may be fit by a power law and that such a scaling relationship may be obtained by assuming that ice fracture is a self-similar process, following a renormalization group method. Zhang et al. (2015) developed a model for the floe size distribution evolution, assuming that all floes of different sizes have the same ITD. The present paper, however, develops a model for the *joint* floe size and thickness distribution, allowing for different ice thickness distribution for each horizontal size class. The Zhang et al. (2015) paper shares many of our goals and we refer to it below, further elaborating on additional differences between the two studies in the treatment of thermodynamics, mechanical interactions, and wave fracturing. Other modeling studies involving the temporal evolution of the floe size distribution have mainly focused on understanding ocean wave propagation and attenuation in the marginal ice zone (Dumont et al., 2011; Williams et al., 2013a, b). These studies developed models of ocean wave propagation, attenuation and associated ice breakage, and modeled the FSD using the renormalization group method of Toyota et al. (2011).

The purpose of the present paper is to develop and demonstrate a framework for modeling the joint distribution of floe sizes and thicknesses (referred to below as the FSTD) $f(r,h)$, with $f(r,h)\ dr\ dh$ being the fraction of the ocean surface area covered by floes of thickness between h and $h+dh$ and lateral size between r and $r+dr$ (a list of variable names and descriptions are provided in Table 1). The ice thickness distribution $g(h)$ and floe size distribution $n(r)$ are obtained by integrating over the joint distribution $f(r,h)$:

$$g(h) = \int_0^\infty f(r,h)dr,$$

$$n(r) = \int_0^\infty f(r,h)dh.$$

The prognostic equation for the joint floe size and thickness distribution has the form

$$\frac{\partial f(\boldsymbol{r})}{\partial t} = -\nabla\cdot(f(\boldsymbol{r})\,\boldsymbol{u}) + \mathcal{L}_\mathrm{T} + \mathcal{L}_\mathrm{M} + \mathcal{L}_\mathrm{W}, \tag{2}$$

where $\boldsymbol{r} = (r,h)$, and $\nabla = (\frac{\partial}{\partial x}, \frac{\partial}{\partial y})$ is the two-dimensional Laplacian. The two-dimensional spatial domain may be thought of as corresponding to a single grid cell of a climate model, on the order of tens of kilometers on a side. The term $\nabla\cdot(f(\boldsymbol{r})\,\boldsymbol{u})$ describes advection of the floe size distribution by the flow of ice. $\mathcal{L}_\mathrm{T}$ is the time rate of change of the floe size distribution due to thermodynamic effects. $\mathcal{L}_\mathrm{M}$ is the time rate of change due to mechanical interaction (rafting and ridging of floes). $\mathcal{L}_\mathrm{W}$ is the time rate of change due to floes being fractured by surface ocean waves. We parameterize each of the above processes, forced by grid-scale atmospheric and oceanic forcing fields. The major contributions of this paper are, first, that it presents the first treatment of the *joint* floe size and thickness distribution. In addition, each of the terms in Eq. (2) as developed below contains a novel formulation of the corresponding process that is physically based and less heuristic than used in previous studies.

The paper proceeds as follows: we first develop explicit representations for the different processes affecting the joint floe size and thickness distribution in response to atmospheric and oceanic forcing in Sect. 2. The model response to individual forcing fields, in the form of air–sea heat fluxes, ice flow that leads to floe collisions, and surface waves, is analyzed in Sect. 3. We conclude in Sect. 4.

2 Representing processes that affect the joint floe size and thickness distribution

2.1 Thermodynamics

Air-sea heat fluxes in the polar oceans lead to the freezing and melting of ice. In regions of open water, cooling produces frazil ice which may consolidate with other floes or form "pancakes". When floes grow due to the accumulation of frazil crystals, or by congelation growth at their bases, their size and thickness will change, but the total number of floes will not. Suppose that the only source or sink of ice volume is due to freezing and melting of existing floes, which causes them to change their size at a rate we denote as G_r and thickness at a rate G_h, and we define $\boldsymbol{G} \equiv (G_\mathrm{r}, G_\mathrm{h})$. Let N be the number distribution, such that $N(\boldsymbol{r})\,dh\,dr$ is the number of floes in the range $(h, h+dh)$, $(r, r+dr)$ (a list of the variables used to describe FSTD thermodynamics is provided in Table 2). The cumulative number distribution is defined as

$$C(\boldsymbol{r}) = \int_0^{\boldsymbol{r}} N(\boldsymbol{r}')\mathrm{d}\boldsymbol{r}' = \int_0^{\boldsymbol{r}} (f(\boldsymbol{r}')/\pi r'^2)\mathrm{d}\boldsymbol{r}',$$

with $\frac{\partial^2}{\partial r\partial h}(C) = N(\boldsymbol{r}) = f(\boldsymbol{r})/\pi r^2$, and it obeys the conservation equation

$$C(\boldsymbol{r},t) = C(\boldsymbol{r} + \boldsymbol{G}\mathrm{d}t, t+\mathrm{d}t),$$

since floes with a finite size and thickness $\boldsymbol{r} = (r,h)$ are, by assumption, neither created nor destroyed by thermodynamic growth and melting. Expanding the right-hand side and rearranging in the limit as $\mathrm{d}t \to 0$ leads to the time rate of change of the cumulative number distribution

$$\frac{\partial C(\boldsymbol{r},t)}{\partial t} = -\,\boldsymbol{G}\cdot\nabla_\mathrm{r} C, \tag{3}$$

where $\nabla_\mathrm{r} = (\frac{\partial}{\partial r}, \frac{\partial}{\partial h})$ is the vector of partial derivatives in (size, thickness) space. Changes to the cumulative number distribution are due to the transfer of ice to larger or smaller sizes by thermodynamic growth and melting. We next make the assumption that thickness changes due to melting and

Table 2. Variables used in the representation of thermodynamical processes in the FSTD model.

Variable	Description	Section
$\mathcal{L}_{\mathrm{T}}$	Thermodynamic component of FSTD model	1
$\boldsymbol{G} = (G_{\mathrm{r}}, G_{\mathrm{h}})$	Ice size and thickness growth rate	2.1
$(r_{\min}, h_{\min})$	Size of smallest ice pancakes	2.1
r_{lw}	Width of lead region	2.1
A_{lead}	Lead area fraction	2.1
Q_{lead}	Lead area heat flux	2.1
Q_{o}	Open water heat flux	2.1
$\dot{A}_{\mathrm{p}}$	Rate of pancake area growth	2.1
$Q_{\mathrm{l,l}}$	Fraction of lead heat flux transmitted to floe sides	2.1
$Q_{\mathrm{l,b}}$	Fraction of lead heat flux transmitted to floe bases	2.1

freezing do not depend on the floe radius, and that horizontal size changes do not depend on the thickness, i.e., $\frac{\partial}{\partial h}(G_{\mathrm{r}}) = \frac{\partial}{\partial r}(G_{\mathrm{h}}) = 0$. The time evolution of the floe size distribution solely due to freezing and melting of existing floes is derived by taking derivatives with respect to both thickness and size of Eq. (3):

$$\left.\frac{\partial f(\boldsymbol{r})}{\partial t}\right|_{\mathrm{melt/freeze}} = -\pi r^2 \frac{\partial}{\partial r}\left(\frac{f(\boldsymbol{r})}{\pi r^2} G_{\mathrm{r}}\right) - \frac{\partial f(\boldsymbol{r})}{\partial h} G_{\mathrm{h}},$$
$$= -\nabla_{\mathrm{r}} \cdot (f(\boldsymbol{r})\boldsymbol{G}) + \frac{2}{r} f(\boldsymbol{r}) G_{\mathrm{r}}. \quad (4)$$

Without loss of generality, consider the interpretation of this equation for the case of freezing in which existing floes get thicker and larger. This implies that some of the area $f(\boldsymbol{r})$ now moves to larger ice classes, represented by the first term in Eq. (4). Note that the integral over all size classes and thickness of the first term vanishes, and therefore it does not describe ice area growth. The total ice area added or removed that belongs to floes of size r, $N(\boldsymbol{r})\mathrm{d} / \mathrm{d}t(\pi r^2)$, equal to $N(\boldsymbol{r})2\pi r\, G_{\mathrm{r}}$, which is equal to the second term in Eq. (4).

Zhang et al. (2015) include the effects of melting and freezing on the FSD, in a way that depends on the lateral growth rate (our G_{r}), but without evaluating this rate in terms of thermodynamic forcing. Their formulation seems to lack the second term on the right-hand side of Eq. (4). The formulation presented here is for the joint FSTD, and therefore depends on both G_{r} and G_{h}. We further evaluate these rates below in terms of air–sea fluxes.

In addition to melting and freezing of existing floes, we must also consider the rate of growth of pancake ice, $\dot{A}_{\mathrm{p}}$, due to the flocculation of frazil crystals in patches of open water away from existing floes. Pancakes are assumed to be created by freezing at the smallest size and thickness accounted for in the model, with an effective radius r_{p} and thickness $h_{\min}$. The full expression for the rate of change of the floe size and thickness distribution due to thermodynamics, $\mathcal{L}_{\mathrm{T}}$, is therefore

$$\mathcal{L}_{\mathrm{T}} = -\nabla_{\mathrm{r}} \cdot (f(\boldsymbol{r})\boldsymbol{G}) + \frac{2}{r} f(\boldsymbol{r}) G_{\mathrm{r}} + \delta(r - r_{\min})\delta(h - h_{\min})\dot{A}_{\mathrm{p}}. \quad (5)$$

The floe size and thickness change rate vector $\boldsymbol{G} = (G_{\mathrm{r}}, G_{\mathrm{h}})$ is determined using the balance of heat fluxes at the ocean–ice–atmosphere interface. Note that our focus here is the impact of thermodynamic forcing on the FSTD: we are not modeling internal ice thermodynamics explicitly. In an application of the FSTD model, a full thermodynamic model of the ocean mixed layer and sea ice would simulate the ice energy budget. Net heat flux in ocean regions adjacent to ice floes (which we refer to as lead regions) is assumed to affect the development of adjacent floes laterally and vertically, while cooling in open water away from existing floes may lead to pancake ice formation (the model does not resolve frazil ice, nor arbitrarily small pancake ice). The lead region is defined as the annulus around each floe of width r_{lw}, and the division of ocean area into lead and open water areas is shown as the blue and white regions in Fig. 1, (see also Parkinson and Washington, 1979). The total lead area, A_{lead}, is approximated as

$$A_{\mathrm{lead}} = \min\left(\int_{\boldsymbol{r}} \left(N(\boldsymbol{r})\pi(r + r_{\mathrm{lw}})^2 - N(\boldsymbol{r})\pi r^2\right)\mathrm{d}\boldsymbol{r}, \phi\right)$$
$$= \min\left(\int_{\boldsymbol{r}} f(\boldsymbol{r})\left(\frac{2r_{\mathrm{lw}}}{r} + \frac{r_{\mathrm{lw}}^2}{r^2}\right)\mathrm{d}\boldsymbol{r}, \phi\right),$$

where ϕ is the open water fraction, and the above integration is over the entire ranges of effective radius and thickness represented in the model. A net air–sea heat flux Q at the ocean surface is therefore partitioned into a lead heat flux $Q_{\mathrm{lead}} = A_{\mathrm{lead}} Q$ and an open water heat flux $Q_o = (\phi - A_{\mathrm{lead}})Q$. If the water is at its freezing point, a cooling heat flux leads to freezing of pancakes of ice of radius $r_{\min}$ and thickness $h_{\min}$, producing the area $\dot{A}_{\mathrm{p}}$ of ice pancakes per unit time where there was formerly open water:

$$\dot{A}_{\mathrm{p}} = \frac{Q_o}{\rho_0 L_f h_{\min}}.$$

The lead region heat flux, Q_{lead}, is further partitioned into a part that leads to basal freezing or melting of existing

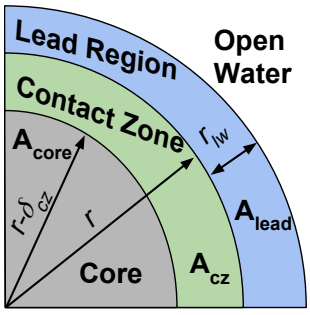

Figure 1. A section of a floe, showing the division of a floe and the surrounding sea surface for the thermodynamic and mechanical interaction components of the FSTD model. The floe itself, of radius r, is divided into the core which is unaffected by ridging and rafting (blue, width $r - \delta_{\mathrm{cz}}$) and contact zone which participates in these interactions (green, width δ_{cz}). The floe is surrounded by the lead region of width r_{lw} where net heat fluxes lead to freezing or melting of the floe itself (blue) and then by open water where cooling may lead to new pancake ice formation (white).

ice floes, $Q_{\mathrm{l,b}}$, and a component that leads to lateral freezing or melting along perimeters of existing floes, $Q_{\mathrm{l,l}}$. Multiple choices for this partitioning are possible, including a binary partition (Washington et al., 1976) with $Q_{\mathrm{l,b}} = Q_{\mathrm{lead}}$, $Q_{\mathrm{l,l}} = 0$ or $Q_{\mathrm{l,l}} = Q_{\mathrm{lead}}$, $Q_{\mathrm{l,b}} = 0$, a parameterization with a quadratic dependence on open water fraction $Q_{\mathrm{l,l}} \propto A_{\mathrm{lead}}^2$ (Parkinson and Washington, 1979), and diffusive and molecular-sublayer parameterizations based on the temperature of the surface waters (Steele, 1992; McPhee, 1992). While these parameterizations have been tested in some detail (Harvey, 1990; Steele, 1992), sensitivity analyses in previous studies have fixed (either explicitly or implicitly) the floe size distribution, and the impact of this assumption on the results is unclear. We choose to simply assume that the lead heat flux is mixed uniformly over the exposed surface of a floe, partitioned according to the ratio of ice basal and lateral surface areas, where it contributes to ice growth or melt. The total fractional lateral surface area (that is, the area of the vertical edges of ice floes, per unit ocean area) is

$$\int_{\boldsymbol{r}} N(\boldsymbol{r}) 2\pi r h \, \mathrm{d}\boldsymbol{r} = \int_{\boldsymbol{r}} f(\boldsymbol{r}) \frac{2h}{r} \, \mathrm{d}\boldsymbol{r} = \overline{2h/r},$$

where N is the number distribution introduced above, $2\pi rh$ is the lateral area of one floe, and $\overline{2h/r}$ represents an average over all ice floes, weighted by the floe size and thickness distribution. The above result depends on the model including an explicit joint FSTD, without which this estimate for the lateral area would not be possible to obtain. The total basal ice surface area per unit ocean area is the ice concentration, c. The partitioning of heat flux from the lead region between the ice base and ice edges is therefore

$$Q_{\mathrm{l,l}} = Q_{\mathrm{lead}} \left(1 + \frac{c}{\overline{2h/r}}\right)^{-1};$$

$$Q_{\mathrm{l,b}} = Q_{\mathrm{lead}} \left(1 + \frac{\overline{2h/r}}{c}\right)^{-1}.$$

The rate of change of ice thickness can be found using a model of ice thermodynamics, given the above-derived open water air–sea flux contribution $Q_{\mathrm{l,b}}$ to the heat budget at the ice base. For example, ignoring ice heat capacity, ice thickness changes due to melting and freezing are related to the net heat flux into the ice from the surface above, Q_{surf} (defined negative upward), and from below (where negative flux means ocean cooling):

$$\rho_i L_{\mathrm{f}} G_{\mathrm{h}} = -(Q_{\mathrm{l,b}} + Q_{\mathrm{surf}}). \tag{6}$$

The rate of change of the lateral floe size is calculated from the corresponding contribution of the air–sea heat flux from the lead region $Q_{\mathrm{l,l}}$:

$$\rho_i L_{\mathrm{f}} G_{\mathrm{r}} = -Q_{\mathrm{l,l}}. \tag{7}$$

The above equations can now be used to express the thermodynamic floe growth rate vector, $\boldsymbol{G} = (G_{\mathrm{r}}, G_{\mathrm{h}})$.

2.2 Mechanical interactions

Wind and ocean currents can drive individual floe collisions, and therefore merge them together. When one floe overrides another while remaining intact, the interaction is referred to as rafting. If the ice at the point of contact disintegrates into a rubble pile, forming a "sail" and a "keel", and the two floes consolidate, the interaction is referred to as ridging. To describe these processes, open water in the floe size and thickness distribution $f(\boldsymbol{r})$ is represented by a delta function at $\boldsymbol{r} = 0$, multiplied by the area fraction of open water. The dynamics of open water formation by ice flows may then be derived by taking integrals over the prognostic Eq. (2) that include or exclude $\boldsymbol{r} = 0$ (a list of the variables used to describe the FSTD response to floe collisions is provided in Table 3). The integral of $f(\boldsymbol{r})$ over all floe sizes and thicknesses, including open water, is equal to 1. Therefore, ignoring thermodynamic and wave effects, we integrate Eq. (2) over a range of floe sizes that include a vanishingly small

Table 3. Variables used in the representation of mechanical interactions in the FSTD model.

Variable	Description	Section
$\mathcal{L}_{\mathrm{M}}$	Mechanical component of FSTD model	1
D_{M}/Dt	Rate of change incorporating ice collisions	2.2
L_{c}	Normalized fraction of concentration lost/gained by collisions	2.2
$\dot{\boldsymbol{\epsilon}}$	Ice flow strain rate tensor	2.2
$\boldsymbol{E}$	Vector of strain rate tensor invariants	2.2
$K(\boldsymbol{r}_1, \boldsymbol{r}_2, \boldsymbol{r})$	Collision kernel: two floes of size $\boldsymbol{r}_1$ and $\boldsymbol{r}_2$, forming a floe of size $\boldsymbol{r}$	2.2
$P_{\mathrm{coll}}(\boldsymbol{r}_1, \boldsymbol{r}_2)$	Probability of two floes of sizes $\boldsymbol{r}_1$ and $\boldsymbol{r}_2$ colliding	2.2
$\delta_{\mathrm{raft/ridge}}$	Width of contact zone for collisions rafting/ridging	2.2
A_{cz}	Area of floe contact zone	2.2
A_{core}	Area of floe core	2.2
$\gamma(h)$	Interpolation coefficient between rafting and ridging	2.2

interval of sizes around $\boldsymbol{r} = (r, h) = \boldsymbol{0}$:

$$\begin{aligned}\int_{\boldsymbol{0}^-} \mathcal{L}_{\mathrm{M}}(\boldsymbol{r})\,\mathrm{d}\boldsymbol{r} &\equiv \lim_{|(\epsilon_1,\epsilon_2)|\to 0} \int_{-\epsilon_1}^{\infty}\int_{-\epsilon_2}^{\infty} \mathcal{L}_{\mathrm{M}}(r,h)\,\mathrm{d}r\,\mathrm{d}h,\\ &= \int_{\boldsymbol{0}^-} \left[\frac{\partial f(\boldsymbol{r})}{\partial t} + \nabla\cdot(f(\boldsymbol{r})\,\boldsymbol{u})\right]\mathrm{d}\boldsymbol{r},\\ &= \frac{\partial 1}{\partial t} + \nabla\cdot(1\,\boldsymbol{u}) = \nabla\cdot\boldsymbol{u}. \qquad (8)\end{aligned}$$

The integral of $f(\boldsymbol{r})$ over all floe sizes and thicknesses, but excluding open water ($\boldsymbol{r} = \boldsymbol{0}$), is equal to the ice concentration, c. Integrating Eq. (2) as before but now excluding $\boldsymbol{r} = \boldsymbol{0}$,

$$\begin{aligned}\int_{\boldsymbol{0}^+} \mathcal{L}_{\mathrm{M}}(\boldsymbol{r})\,\mathrm{d}\boldsymbol{r} &\equiv \lim_{|(\epsilon_1,\epsilon_2)|\to 0} \int_{\epsilon_1}^{\infty}\int_{\epsilon_2}^{\infty} \mathcal{L}_{\mathrm{M}}(r,h)\,\mathrm{d}r\,\mathrm{d}h,\\ &= \int_{\boldsymbol{0}^+} \left[\frac{\partial f(\boldsymbol{r})}{\partial t} + \nabla\cdot(f(\boldsymbol{r})\,\boldsymbol{u})\right]\mathrm{d}\boldsymbol{r},\\ &= \frac{\partial c}{\partial t} + \boldsymbol{u}\cdot\nabla c + c(\nabla\cdot\boldsymbol{u}) \equiv \frac{D_{\mathrm{M}}c}{Dt}. \qquad (9)\end{aligned}$$

The above definition of the operator D_{M}/Dt implies that $D_{\mathrm{M}}(1)/Dt = \nabla\cdot\boldsymbol{u}$. The subscript M indicates that this operator represents concentration changes due to mechanical interactions only. $\frac{D_{\mathrm{M}}c}{Dt}$ is equal to the total sea-ice area which is eliminated due to the collisions of floes per unit of time. Subtracting Eq. (8) from Eq. (9),

$$\int_{\boldsymbol{0}^-}^{\boldsymbol{0}^+} \mathcal{L}_{\mathrm{M}}(\boldsymbol{r})\,\mathrm{d}\boldsymbol{r} = \nabla\cdot\boldsymbol{u} - \frac{D_{\mathrm{M}}c}{Dt}.$$

This result implies that $\mathcal{L}_{\mathrm{M}}(\boldsymbol{r})$ has a $\delta(\boldsymbol{r})$ component due to open water creation in floe collisions, or the integral on the infinitesimally small range near size zero would have vanished. Note that the function $\delta(\boldsymbol{r})$ is the two-dimensional delta function: $\delta(\boldsymbol{r}) = \delta([r,h]) \equiv \delta(r)\delta(h)$.

Equation (9) suggests that there should be another term in $\mathcal{L}_{\mathrm{M}}(\boldsymbol{r})$ that, when integrated over all sizes, leads to $\frac{D_{\mathrm{M}}c}{Dt}$. This suggests the following form:

$$\mathcal{L}_{\mathrm{M}} = (\nabla\cdot\boldsymbol{u})\delta(\boldsymbol{r}) + \frac{D_{\mathrm{M}}c}{Dt}\left[L_{\mathrm{c}}(\boldsymbol{r}) - \delta(\boldsymbol{r})\right], \qquad (10)$$

where $L_{\mathrm{c}}(\boldsymbol{r})$ is yet unspecified except that its integral over all sizes is 1, and it is non-singular at $||\boldsymbol{r}|| = 0$:

$$\int_{\boldsymbol{0}^+} L_{\mathrm{c}}(\boldsymbol{r})\;\mathrm{d}\boldsymbol{r} = \int_{\boldsymbol{0}^-} L_{\mathrm{c}}(\boldsymbol{r})\;\mathrm{d}\boldsymbol{r} = 1. \qquad (11)$$

The factor $L_{\mathrm{c}}(\boldsymbol{r})$ quantifies the relative fraction of the total concentration lost due to collisions at each floe size. The terms in Eq. (10) that are proportional to $\delta(\boldsymbol{r})$ represent together the formation of open water due to collisions driven by divergent ice motions. The remaining term represents the rearrangement of ice area among floe classes. It remains to derive expressions for the rate of open water formation due to collisions $\frac{D_{\mathrm{M}}c}{Dt}$, and the rearrangement of the floe size and thickness distribution in response to a unit amount of open water formation due to collisions, $L_{\mathrm{c}}(\boldsymbol{r})$.

Thorndike et al. (1975) described the rate of mechanical interactions as depending on the divergence, convergence, and shear of the ice flow, weighted by the relative size of the invariants of the ice strain rate tensor $\dot{\boldsymbol{\epsilon}}$:

$$\dot{\boldsymbol{\epsilon}}_{ij} = \frac{1}{2}\left(\frac{\partial u_i}{\partial x_j} + \frac{\partial u_j}{\partial x_i}\right). \qquad (12)$$

Defining the deviatoric strain tensor, $\dot{\boldsymbol{\epsilon}}'_{ij} = \dot{\boldsymbol{\epsilon}}_{ij} - \delta_{ij}\nabla\cdot\boldsymbol{u}/2$, equal to the divergence-free part of $\dot{\boldsymbol{\epsilon}}_{ij}$, two relevant invariants may be written as $\boldsymbol{E} = (\epsilon_{\mathrm{I}}, \epsilon_{\mathrm{II}}) = (\nabla\cdot\boldsymbol{u}, 2|-\dot{\boldsymbol{\epsilon}}'|^{1/2})$. The first invariant is the flow divergence and the second is calculated from the determinant of the deviatoric strain rate tensor, and is equal to the maximal shear strain rate. Given these definitions, we parameterize the rate of ice area loss due to collisions as

$$\frac{D_{\mathrm{M}}c}{Dt} = \frac{1}{2}\left(\epsilon_{\mathrm{I}} - ||\boldsymbol{E}||\right) \le 0, \qquad (13)$$

which allows us to write the mechanical interaction term in the FSTD equation as

$$\mathcal{L}_{\mathrm{M}} = \delta(\boldsymbol{r})\epsilon_{\mathrm{I}} + \frac{1}{2}\left(||\boldsymbol{E}|| - \epsilon_{\mathrm{I}}\right)\left[\delta(\boldsymbol{r}) - L_{\mathrm{c}}\right]. \tag{14}$$

This formulation is exactly equivalent to that of Thorndike et al. (1975); see Appendix for details. In the case of ice flow characterized by pure divergence, $\boldsymbol{E} = (\nabla\cdot\boldsymbol{u}, 0)$ and $\nabla\cdot\boldsymbol{u} > 0$, the mechanical interactions are represented as a delta function at $\boldsymbol{r} = 0$, representing only the formation of open water by divergent ice flow. In pure convergence, $\boldsymbol{E} = (\nabla\cdot\boldsymbol{u}, 0)$ and $\nabla\cdot\boldsymbol{u} < 0$, and mechanical interactions create open water through collisions and $\mathcal{L}_{\mathrm{M}}(\boldsymbol{r}) = |\nabla\cdot\boldsymbol{u}|L_{\mathrm{c}}(\boldsymbol{r})$. When the ice flow is characterized by shear motions, $||\boldsymbol{E}|| = \epsilon_{\mathrm{II}}$, and collisions still occur due to the differential motion of neighboring floes, which forms open water at a rate of $\frac{D_{\mathrm{M}}c}{Dt} = \epsilon_{\mathrm{II}}/2$ per second. Other choices of $\frac{D_{\mathrm{M}}c}{Dt}$ could satisfy Eq. (10), but the Thorndike parameterization meets the intuitive requirements that in pure divergence no collisions occur, while in pure convergence they do, and in pure shear, collisions occur such that the rate of open water formation per unit strain is reduced relative to the case of pure convergence.

The effects of mechanical interactions on the FSD are represented by Zhang et al. (2015) similarly to Eq. (10), with the rate of area loss (our $\frac{D_{\mathrm{M}}c}{Dt}$) taken from Hibler III (1980), and assuming that all floes of different sizes have the same ITD. In our joint FSTD formulation, the mechanical interactions are represented for floes characterized by both specific thickness and specific size. Here, interactions between floes are treated as binary collisions, and our model does not consider multiple simultaneous collisions in a single time step. Such multiple collisions lead to clustering, which is relevant for granular media undergoing deformation (Shen and Sankaran, 2004), with sea ice being a possible example. However, Herman (2013) demonstrated in numerical simulations that floes may also aggregate into clusters via a sequence of binary interactions between pairs of floes.

The rearrangement of floe area in response to a unit amount of open water formation, $L_{\mathrm{c}}(\boldsymbol{r})$, is represented using a collision kernel $K(\boldsymbol{r}_1, \boldsymbol{r}_2; \boldsymbol{r})$. Let $K(\boldsymbol{r}_1, \boldsymbol{r}_2; \boldsymbol{r})\,\mathrm{d}\boldsymbol{r}_1\,\mathrm{d}\boldsymbol{r}_2\,\mathrm{d}\boldsymbol{r}$ be equal to the number of collisions per unit time between floes in the range $(\boldsymbol{r}_1, \boldsymbol{r}_1 + \mathrm{d}\boldsymbol{r}_1)$ and floes in the range $(\boldsymbol{r}_2, \boldsymbol{r}_2 + \mathrm{d}\boldsymbol{r}_2)$, that form floes in the range $(\boldsymbol{r}, \boldsymbol{r} + \mathrm{d}\boldsymbol{r})$, per unit area of open water formation. In general, the floe number distribution subject to mechanical combination of floes evolves according to

$$\frac{\partial N(\boldsymbol{r})}{\partial t} = \int_{\boldsymbol{r}_1}\int_{\boldsymbol{r}_2}\Bigg[\frac{1}{2}N(\boldsymbol{r}_1)N(\boldsymbol{r}_2)K(\boldsymbol{r}_1, \boldsymbol{r}_2; \boldsymbol{r}) - N(\boldsymbol{r})N(\boldsymbol{r}_2)K(\boldsymbol{r}, \boldsymbol{r}_2; \boldsymbol{r}_1)\Bigg]\mathrm{d}\boldsymbol{r}_1\,\mathrm{d}\boldsymbol{r}_2, \tag{15}$$

where the notation $\int_{\boldsymbol{r}}\mathrm{d}\boldsymbol{r}$ is taken to mean an integral over all floe sizes and thicknesses resolved by the model. The factor of $1/2$ prevents double-counting: since K is symmetric with respect to its first two arguments, each interaction pair $(\boldsymbol{r}_1, \boldsymbol{r}_2)$ is counted twice in the integral in Eq. (15). This represents the rate of change in the number of floes of size $\boldsymbol{r}_3$ due to mechanical interactions. In reality, some floe collisions may lead to a rebound and erosion of floe edges rather than to a merging of the floes, yet we do not account for such a process. The first term on the right-hand side of Eq. (15) represents the increase in floe number at size $\boldsymbol{r}$ due to collisions between floes of other sizes, and the second term represents the loss in floe number at size $\boldsymbol{r}$ due to combination of floes of size $\boldsymbol{r}$ with other floes. Equation (15) is a generalization of the Smoluchowski coagulation equation that has been previously used to model the sea-ice thickness distribution (Godlovitch et al., 2011). If we multiply Eq. (15) by the area of a floe of size $\boldsymbol{r}$, we obtain the rate of change of the fractional area covered by floes of size $\boldsymbol{r}$ due to mechanical interactions, which is nothing but the definition of $\mathcal{L}_{\mathrm{M}}(\boldsymbol{r})$:

$$\frac{\partial f(\boldsymbol{r})}{\partial t} = (\pi r^2)\frac{\partial N(\boldsymbol{r})}{\partial t} = \mathcal{L}_{\mathrm{M}}(\boldsymbol{r});\ (r \neq 0). \tag{16}$$

We have already concluded above that away from $\boldsymbol{r} = 0$ we have $\mathcal{L}_{\mathrm{M}}(\boldsymbol{r}) = L_{\mathrm{c}}(\boldsymbol{r})$. Therefore the above equation gives

$$L_{\mathrm{c}}(\boldsymbol{r}) = (\pi r^2)\frac{\partial N(\boldsymbol{r})}{\partial t}, \tag{17}$$

where $\partial N/\partial t$ is taken from Eq. (15). We represent the kernel $K(\boldsymbol{r}_1, \boldsymbol{r}_2, \boldsymbol{r})$ as the product of two factors. The first is the probability of collision via ridging or rafting of two floes of size $\boldsymbol{r}_1$ and $\boldsymbol{r}_2$, termed $P_{\mathrm{coll}}(\boldsymbol{r}_1, \boldsymbol{r}_2)$ where the subscript "coll" is either "ridge" or "raft", and the probabilities are to be defined more specifically shortly.

The second factor is a delta function, $\delta(\boldsymbol{r} - \mathrm{R}(\boldsymbol{r}_1, \boldsymbol{r}_2))$, that limits the pairs of collision partners to only those that form a floe of size $\boldsymbol{r} = \mathrm{R}(\boldsymbol{r}_1, \boldsymbol{r}_2)$, specified below, and whose area is smaller than the area of the two colliding floes combined. Noting again that the number distribution and area distribution are related through $N(\boldsymbol{r}) = \pi r^2 f(\boldsymbol{r})$, we combine Eq. (17) and (15) to find

$$L_{\mathrm{c}}(\boldsymbol{r}) = L_{\mathrm{c}}^{*}\iint_{\boldsymbol{r}_1,\boldsymbol{r}_2}\Bigg[\frac{1}{2}\frac{r^2}{\pi r_1^2 r_2^2}f(\boldsymbol{r}_1)f(\boldsymbol{r}_2)\mathrm{P}_{\mathrm{coll}}(\boldsymbol{r}_1, \boldsymbol{r}_2)\delta(\boldsymbol{r} - \mathrm{R}(\boldsymbol{r}_1, \boldsymbol{r}_2)) - \frac{1}{\pi r_2^2}f(\boldsymbol{r})f(\boldsymbol{r}_2)\mathrm{P}_{\mathrm{coll}}(\boldsymbol{r}, \boldsymbol{r}_2)\delta(\boldsymbol{r}_1 - \mathrm{R}(\boldsymbol{r}, \boldsymbol{r}_2))\Bigg]\mathrm{d}\boldsymbol{r}_1\mathrm{d}\boldsymbol{r}_2. \tag{18}$$

The coefficient L_{c}^{*} is a normalization constant ensuring that the integral over $L_{\mathrm{c}}(\boldsymbol{r})$ is 1 (Eq. 11). In the discretized version of Eq. (18), two floe classes of discrete size $\boldsymbol{r}_1^{\mathrm{d}}$ and $\boldsymbol{r}_2^{\mathrm{d}}$ which combine to form floes of discrete size $\boldsymbol{r}^{\mathrm{d}}$ do not necessarily satisfy $\pi(r_1^{\mathrm{d}})^2 h_1^{\mathrm{d}} + \pi(r_2^{\mathrm{d}})^2 h_2^{\mathrm{d}} = \pi(r^{\mathrm{d}})^2 h^{\mathrm{d}}$. Ice volume conservation that is independent of the discretization is achieved by determining the newly formed area of the new floes, in each time step, using the constraint that volume must be conserved:

$$\Delta f(\boldsymbol{r}_1^{\mathrm{d}})h_1^{\mathrm{d}} + \Delta f(\boldsymbol{r}_2^{\mathrm{d}})h_2^{\mathrm{d}} = -\Delta f(\boldsymbol{r}^{\mathrm{d}})h^{\mathrm{d}},$$

where $\Delta f(\boldsymbol{r})$ is the area change at size $\boldsymbol{r}$ in a single time step due to the mechanical interaction considered here. Thus the total volume lost by floes at size $\boldsymbol{r}_1^{\mathrm{d}}$ and $\boldsymbol{r}_2^{\mathrm{d}}$ (left-hand side) is equal to the corresponding volume gained at size $\boldsymbol{r}_3^{\mathrm{d}}$ (right-hand side).

2.2.1 Probability of collision

We choose the functions $\mathrm{P}_{\mathrm{coll}}(\boldsymbol{r}_1, \boldsymbol{r}_2)$ to be proportional to the probability that two floes of size $\boldsymbol{r}_1$ and $\boldsymbol{r}_2$ will overlap if placed randomly in the domain, and they are calculated in a similar manner for both mechanical processes (rafting or ridging). We consider such an overlap as an indication that mechanical interaction has occurred. The area of each floe that may be deformed due to mechanical interactions is restricted to a small region near the edge of the floe, represented in our model by a narrow annulus, which we term a "contact zone", of width $\delta_{\mathrm{cz}} = \delta_{\mathrm{ridge}}$ or $\delta_{\mathrm{cz}} = \delta_{\mathrm{raft}}$ at the floe edge, which depends on the floe size and the interaction type; we also term the interiors of floes "cores" (Fig. 1). The area of a single floe of size s is therefore broken down as

$$\pi s^2 = A_{\mathrm{core}}(s) + A_{\mathrm{cz}}(s) = \pi(s - \delta_{\mathrm{cz}})^2 + \pi(2\delta_{\mathrm{cz}} s - \delta_{\mathrm{cz}}^2).$$

The above-defined probability of collision between floes of size r_1 and r_2 is proportional to the product of contact zone areas divided by the open ocean area, A, not including the core areas:

$$\mathrm{P}_{\mathrm{coll}}(\boldsymbol{r}_1, \boldsymbol{r}_2) \propto \frac{A_{\mathrm{cz}}(r_1) A_{\mathrm{cz}}(r_2)}{(A - A_{\mathrm{core}}(r_1) - A_{\mathrm{core}}(r_2))^2}.$$

The above probability that two floes will collide is based on geometric constraints. However, the rate of collisions depends also on the ice strain rate tensor $\dot{\boldsymbol{\epsilon}}$ as explained above, and this tensor depends on external forcings such as the strength of the prevailing winds and currents (Shen et al., 1987; Herman, 2011, 2013; Bennetts and Williams, 2015), but the determination of that relationship is not a focus of the FSTD model presented here.

Data of the morphology and width distribution of ridges and rafts as a function of the size of the combining ice floes are scarce, though there are indications that rafts can be substantially larger than ridges (Hopkins et al., 1999). We crudely define the width of the contact zone in ridging to be 5 m, or the size of the smaller of the two combining floes, whichever is smaller:

$$\delta_{\mathrm{ridge}}(r_1, r_2) = \min(5\,\mathrm{m}, r_1, r_2).$$

For rafting, we assume a larger portion of the smaller floe may be uplifted, up to 10 m:

$$\delta_{\mathrm{raft}}(r_1, r_2) = \min(10\,\mathrm{m}, r_1, r_2).$$

Both choices lead to larger ridges and rafts as the size of the interacting floes increases. Given observations of these processes, one can refine the above choices, to which our model is not overly sensitive. Finally, we assume that ridging occurs for floes thicker than 0.3 m, and rafting occurs when both floes are thinner than 0.3 m, consistent with the study of Parmerter (1975), with a smooth transition between the two regimes implemented by a coefficient $\gamma(h)$ which tends to 1 for thicknesses that are prone to rafting and to 0 for ridging:

$$K(\boldsymbol{r}_1, \boldsymbol{r}_2; \boldsymbol{r}) = \gamma(h_1)\gamma(h_2)\mathrm{P}_{\mathrm{raft}}(\boldsymbol{r}_1, \boldsymbol{r}_2)\delta(\boldsymbol{r} - \mathrm{R}_{\mathrm{raft}}(\boldsymbol{r}_1, \boldsymbol{r}_2)) + (1 - \gamma(h_1)\gamma(h_2))\mathrm{P}_{\mathrm{ridge}}(\boldsymbol{r}_1, \boldsymbol{r}_2)\delta(\boldsymbol{r} - \mathrm{R}_{\mathrm{ridge}}(\boldsymbol{r}_1, \boldsymbol{r}_2)),$$

$$\gamma(h) = \frac{1}{2} - \frac{1}{2}\tanh\left[(h - 0.3)/0.05\right].$$

2.2.2 New floe size

The ice area lost in an interaction is different for rafting and ridging. In rafting, the entire contact zone is replaced by ice whose thickness is the sum of that of the original floes. In ridging, the contact zone is increased in thickness by a factor of 5, compressing its area by a factor of 1/5 (Parmerter and Coon, 1972). Given that our model assumes each floe has a uniform thickness, we treat floes formed by ridging or rafting to be of uniform thickness, chosen to conserve volume. This choice eliminates the need for keeping track of sea-ice morphology. Observations (Collins et al., 2015; Kohout et al., 2015) have indicated that floes may break up along ridges, in which case Eq. (18) may be used to provide information about the ridge density. This is a potential future extension of the present work.

Assuming without loss of generality that $r_1 \le r_2$, the area of the newly formed floes is therefore given by the sum of the areas minus the area lost to either ridging or rafting. We then divide this area by π and take the square root to find the size of the newly formed floes. The thickness of the formed floe is calculated from volume conservation. We therefore have

$$[r, h] = R([r_1, h_1], [r_2, h_2])_{\mathrm{raft}} = \left(\sqrt{r_1^2 + r_2^2 - \frac{1}{2}A_{\mathrm{cz,raft}}(r_1)/\pi},\ \frac{V(\boldsymbol{r_1}) + V(\boldsymbol{r_2})}{\pi r^2}\right),$$

$$[r, h] = R([r_1, h_1], [r_2, h_2])_{\mathrm{ridge}} = \left(\sqrt{r_1^2 + r_2^2 - \frac{4}{5}A_{\mathrm{cz,ridge}}(r_1)/\pi},\ \frac{V(\boldsymbol{r_1}) + V(\boldsymbol{r_2})}{\pi r^2}\right),$$

where $V(\boldsymbol{r}) = V([r, h]) = h\pi r^2$ is the volume of an ice floe.

2.3 Swell fracture

Sea surface height variations due to surface ocean waves strain and possibly break sea-ice floes into smaller floes of varying sizes. Since this process does not create or destroy sea-ice area, the response of the FSTD to the fracture of sea ice by waves obeys the conservation law

$$\int_{\mathrm{r}} \mathcal{L}_W(\boldsymbol{r})\mathrm{d}\boldsymbol{r} = 0,$$

Table 4. Variables used in the representation of the fracture of ice by surface waves in the FSTD model.

Variable	Description	Section
$\mathcal{L}_W$	Ice fracture component of FSTD model	1
$\Omega(\boldsymbol{r},t)$	Area of floes of size $\boldsymbol{r}$ fractured by waves	2.3
$F(\boldsymbol{r},\boldsymbol{s})$	Floe size and thickness distribution of new floes formed by the fracture of floes of size $\boldsymbol{r}$ by waves	2.3
$\alpha(\lambda,h)$	Attenuation coefficient (per floe) for waves of wavelength λ encountering ice of thickness h	2.3
D	Width of computational domain onto which waves are incident	2.3
$S(\lambda)$	Incident wave spectrum	2.3
$\eta(x)$	Sea surface height record	2.3
ϕ_i	Phase of ith component of sea surface height Fourier spectrum	2.3
$a(\lambda_i)$	amplitude of ith component of sea surface height Fourier spectrum	2.3
ϵ_{crit}	Critical strain rate for breaking of floes	2.3
H_{s}	Significant wave height (height of 1/3 highest waves)	2.3
X^*	Collection of potential fracture lengths	2.3
$R(r,h)$	Histogram of lengths that lead to fracture of ice of thickness h	2.3
λ_z	Wavelength corresponding to zero-crossing period	2.3
c_{g}	Group velocity of waves of wavelength λ to cross domain	2.3
T_z	Zero-crossing period for wave record	3

where $\mathcal{L}_W(\boldsymbol{r})$ is the time rate of change of floes of size and thickness $\boldsymbol{r}=(r,h)$ due to the fracture of ice by surface waves in Eq. 2, and the integral is over all sizes and thicknesses (a list of the variables used to describe the response of the FSTD to ice fracture by waves is provided in Table 4). Suppose that an area of floes $\Omega(\boldsymbol{r},t)\,\mathrm{d}\boldsymbol{r}$ with sizes between $\boldsymbol{r}$ and $\boldsymbol{r}+\mathrm{d}\boldsymbol{r}$ is fractured per unit time. Let new floes resulting from this process have the floe size distribution $F(\boldsymbol{r},\boldsymbol{s})\,d\boldsymbol{s}$, equal to the fraction of $\Omega(\boldsymbol{r},t)$ that becomes floes with size between $\boldsymbol{s}$ and $\boldsymbol{s}+d\boldsymbol{s}$. The rate of change of area of floes of size $\boldsymbol{r}$ due to fracture by ocean surface waves is then

$$\mathcal{L}_W(\boldsymbol{r}) = -\Omega(\boldsymbol{r},t) + \int_{\boldsymbol{s}} \Omega(\boldsymbol{s},t)F(\boldsymbol{s},\boldsymbol{r})\mathrm{d}\boldsymbol{s}. \tag{19}$$

The first term is the loss of fractional area of size $\boldsymbol{r}$ that is fractured per unit time, and the second is the increase in the area occupied by floes of size $\boldsymbol{r}$ due to the fracture of floes of larger sizes.

Kohout and Meylan (2008) modeled floes as long floating elastic plates, and showed ocean surface waves to be attenuated exponentially as a function of the number, Λ, of ice floes the waves encounter as they propagate into an ice pack. Wave energy therefore decays as $\exp(-\alpha\Lambda)$, where the attenuation coefficient is $\alpha(T,\bar{h})$, T is the wave period, and $\bar{h}$ the mean ice thickness. We approximate the number of floes per unit distance as $c(2\bar{r})^{-1}$, where c is the ice concentration and $\bar{r}$ the average effective radius, and approximate this attenuation by fitting the attenuation coefficient $\alpha(T,\bar{h})$ calculated by Kohout and Meylan (2008) (their Fig. 6) to a quadratic function of the period and mean thickness (Fig. 2). Kohout and Meylan (2008) only report an attenuation coefficient for wave periods longer than 6 s and thicknesses less than 3 m (red box in Fig. 2), so we extrapolate to shorter periods and higher thicknesses using this fit when necessary. We convert

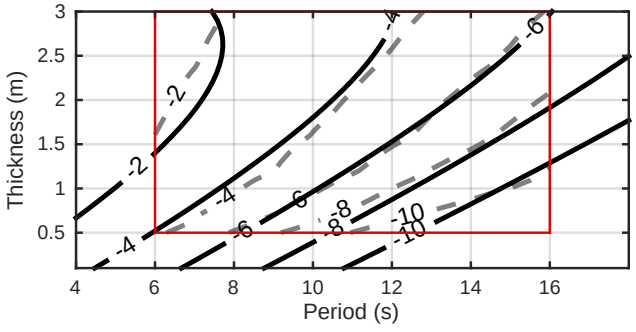

Figure 2. The natural logarithm of the attenuation coefficient α calculated by Kohout and Meylan (2008) (dashes, inside the red box) and a quadratic fit to this attenuation coefficient that is used in Sect. 2.3 (solid lines). Solid contours outside of the red box are extrapolated using the quadratic fit. The fit is given by $\ln\alpha(T,\bar{h}) = -0.3203+2.058\bar{h}-0.9375T-0.4269\bar{h}^2+0.1566\bar{h}T+0.0006T^2$.

the attenuation coefficients from a function of wave period to a function of wavelength using the deep-water surface gravity wave dispersion relation $\lambda = gT^2/2\pi$.

Scattering models may under-predict attenuation rates (Williams et al., 2013b), which may allow for longer penetration of waves into the MIZ than is physically realistic. Updated models of the wave attenuation (Bennetts and Squire, 2012) suggest different attenuation coefficients as a function of wave period and ice thickness. We tested our model with the Bennetts and Squire (2012) attenuation coefficient, and show in the Supplement (Sect. S1.4) that our FSTD model can be sensitive to the choice of attenuation model. Future applications of this FSTD model should therefore carefully consider the wave attenuation formulation, based on both model estimates and observations (e.g., Meylan et al., 2014).

We determine the floe size distribution caused by the fracture of ice of size $\boldsymbol{s}$ by surface waves, $F(\boldsymbol{s},\boldsymbol{r})\mathrm{d}\boldsymbol{r}$, based on the wave spectrum $S(\lambda)$ (in units of meters, see Bouws et al., 1998, p. 11), which is equal to the wave energy spectrum normalized by ρg. Williams et al. (2013a) used a Rayleigh distribution for the strain spectrum to predict breaking of floes; however this does not determine the floe sizes produced by the breaking, which we address as follows. First, the continuous spectrum and attenuation coefficients are used to generate realizations of the sea surface height. Next, these realizations are used to calculate the strain applied to the ice floes. Finally, a statistical distribution of resulting floe size is calculated from the sea surface height plus a critical strain condition. Details of this procedure follow, and are demonstrated in detail in the supplementary material section S3.

We consider for simplicity a one-dimensional domain and assume that floes flex with the sea surface height field $\eta(x)$, experiencing a strain $\epsilon = \frac{h}{2}\frac{\partial^2\eta}{\partial x^2}$ (Dumont et al., 2011, p. 4). If the maximum strain, which occurs at the trough and crest of a wave, exceeds an empirically defined value ϵ_{crit}, the floe will break. For a monochromatic swell wave of wavelength λ, this leads to floes of size $\lambda/2$. For a discretization into N_λ spectral lines with spacing $\Delta\lambda$, spectral amplitudes are defined as $a_i = \sqrt{2S(\lambda_i)\Delta\lambda}$, so that $\int S(\lambda)d\lambda \approx \sum_{i=1}^{N_\lambda} S(\lambda)\Delta\lambda = \sum_{i=1}^{N_\lambda} a_i^2/2$. Let the width of the domain to which the FSTD model is applied be D (e.g., the width of a GCM grid cell which borders on open water). A realization of the sea surface height $\eta(x)$ is generated according to

$$\eta(x_j) = \sum_{i=1}^{N_\lambda} a_i e^{-\alpha(\lambda_i)x_j}\cos\left(\frac{2\pi x_j}{\lambda_i} + \phi_i\right), \tag{20}$$

where x ranges from 0 to D, the random phases ϕ_i are drawn from a uniform distribution between 0 and 2π, and $\alpha(\lambda_i)$ is the attenuation coefficient for waves of wavelength λ_i.

If the strain is calculated locally from $\eta(x)$, the critical strain is reached almost everywhere for a realistically generated wave field (see the Supplement, Fig. S10). Instead, a floe is assumed to fracture when it is strained between three successive local extrema of η, where points are defined to be extrema if they are a local maximum or minimum over a distance of 10 m on both sides, based on the observations of Toyota et al. (2011) who find this to be the order of the smallest floe size affected by wave fracture. For a triplet of successive extrema (max, min, max; or min, max, min) of η, $(x_{i-1}^*, x_i^*, x_i^*)$, the strain felt by the floe at x_i^* is calculated by a finite difference approximation (see the Supplement, Sect. S3). When the magnitude of this strain exceeds the critical strain, $\epsilon_{\mathrm{crit}} = 3\times10^{-5}$, the floe will break. This determines a set of points at which a floe of thickness h will fracture, $X_i^*(h)$. From this set of points we define the size of the fractured floe as $X_{i+1}^* - X_i^*$. We form a histogram $R(r,h)$ of the number of occurrences of each fracture of size r, which is normalized so that $\int rR(r,h_\mathrm{s})\,\mathrm{d}r = D$. In this way, $R(r,h_\mathrm{s})\mathrm{d}r$ is equal to the number of fractures with size between r and $r+\mathrm{d}r$ and thickness h_s when waves affect a fully ice-covered domain of length D. We assume that a floe of size s will fracture only when $X_{i+1}^* - X_i^* = r < s$, and that the number of fractures of size r is either proportional to $R(r)$ (for $r<s$), or 0 (for $r>=s$). The total length of fractures of size r is thus proportional to $rR(r)$, or 0, for $r>s$. The floe size distribution formed by the fracture of a floe of size s, $F(\boldsymbol{s},\boldsymbol{r})$ is therefore equal to the total length of floes of size r that are formed by this fracturing of a floe of size s, normalized such that $\int_0^\infty F(\boldsymbol{s},\boldsymbol{r})\mathrm{d}\boldsymbol{r} = 1$, i.e.,

$$F(\boldsymbol{s},\boldsymbol{r}) = F([s,h_\mathrm{s}],[r,h]) = \frac{rR(r,h_\mathrm{s})}{\int_0^s rR(r,h_\mathrm{s})dr}\delta(h-h_\mathrm{s}). \tag{21}$$

The upper limit of the normalization integral in the denominator is truncated to s because the integrand vanishes for larger values of r as explained above. The delta function $\delta(h-h_\mathrm{s})$ represents the fact that fracture does not change ice thickness, i.e., any floes formed from the fracture of ice with thickness h_s will also have thickness h_s.

The function $\Omega(\boldsymbol{r},t)\mathrm{d}\boldsymbol{r}$ is the fractional area that belongs to floes of size between $\boldsymbol{r}$ and $\boldsymbol{r}+\mathrm{d}\boldsymbol{r}$ that is fractured per unit time. It is set equal to the the area fraction covered by floes of size $\boldsymbol{r}$, f($\boldsymbol{r}$), multiplied by the fraction of the domain reached by waves of group velocity c_g per unit time, c_g/D, multiplied by the probability that floes of size $\boldsymbol{r}$ will fracture by waves. To calculate this probability, we note that $r'R(r')$ is the total length of the domain covered by waves that can break floes into size r'. Integrating this over r' from 0 to a size r, we find the total width of the domain covered by waves that can produce floes smaller than r, which is the same as the length of the domain covered with waves that can break floes of size r into smaller sizes. Normalizing by the domain width D, we find the final factor in the expression for Ω:

$$\Omega([r,h],t) = f(\boldsymbol{r})(c_\mathrm{g}/D)\left(\int_0^r r'R(r',h)dr'/D\right). \tag{22}$$

The group velocity is taken to be that of the mean zero-crossing wavelength, $c_\mathrm{g} = \sqrt{\frac{\lambda_{zg}}{8\pi}}$. Observations of wave propagation in ice (Collins et al., 2015) have suggested that the propagation speed of fracture in ice may be slower than the group velocity of surface waves. With more data, the above choice for c_g may be re-evaluated.

The effects of the fracture of ice by waves on the FSD is represented by Zhang et al. (2015) based on an expression similar to Eq. (19), assuming that only floes with horizontal size larger than a specified threshold break, that a fractured floe is equally likely to form any smaller size within a specified range, and that all floes in a given size class have the same ITD. In the representation in the present paper of the effects of ice fracture by waves on the joint FSTD, the wave spectrum plays a central role in determining the resulting floe

sizes, as well as the propagation distance over which ocean waves are attenuated by the ice field. Information about the specific thickness of individual floe sizes informs the strain rate failure criterion and therefore determines which floes will be fractured.

3 Model results

To demonstrate and understand the model's response to a variety of forcing scenarios, we first examine its response over a single time step in three runs with idealized forcing fields. Each of these scenarios applies one of the following forcing fields: a net surface cooling $Q = -100\,\mathrm{W\,m^{-2}}$ which induces ice growth, a rate of ice flow convergence of $\nabla \cdot \boldsymbol{u} = -5 \times 10^{-9}\,\mathrm{s^{-1}}$ which induces floe collisions, and a surface gravity wave field of a single wavelength $\lambda = 56\,\mathrm{m}$ and amplitude of 1 m, leading to ice fracture. The model is initialized with a size and thickness distribution composed of two Gaussian peaks (Fig. 3a). The first (referred to as size I below) has a mean size of 90 m and a mean thickness of 0.25 m. Ice at this size and thickness is susceptible to fracture by surface waves and rafting. The second peak (size II) has a mean size of 15 m and a mean thickness 1.5 m. Ice at this size and thickness tends to ridge rather than raft, and is not susceptible to fracture given our specified wave field. This second point is important, as it demonstrates a possible scenario in which knowledge of the ITD and FSD, separately, would not be sufficient to evolve the FSTD, as some floes, independent of their thickness, will not fracture. The initial sea-ice concentration is 75 %. The domain width is $D = 10\,\mathrm{km}$, and the width of the lead region is set to be $r_{\mathrm{lw}} = r_{\mathrm{min}} = 0.5\,\mathrm{m}$, the smallest floe size resolved in this model. The critical strain amplitude for flexural failure, ϵ_{crit}, is set to 3×10^{-5} in line with other studies (Kohout and Meylan, 2008; Dumont et al., 2011). Williams et al. (2013a) formulated a more complex expression for the critical failure limit, and this was found to have a significant effect on wave fracturing (Williams et al., 2013b). We examine the model sensitivity to some of the main parameters used in these model simulations in the Supplement (Sect. S1).

When two floes of size r and s combine due to rafting or riding interactions, they form a new floe with effective radius $r' > \max(r, s)$. For an arbitrary floe size discretization into size bins, this new size may not lie within a bin representing a size larger than those of the two interacting floes. As a result, interacting floes may accumulate at a single bin size rather than move into bins representing larger sizes. The minimum bin resolution necessary to avoid this problem is set by the interaction of two floes that are the same size r, with r smaller than the ridge width δ_{ridge}. When two such small floes interact via ridging in our model, one of them becomes 5 times thicker and its area is reduced by a factor of 5. They therefore form a floe of size $\sqrt{6/5}r$. We select a variable discretization, with $r_{n+1} = \sqrt{6/5}r_n$, with 64 floe sizes between 0.5 and 156 m. There are 14 thickness categories, 13 of which are equally spaced between 0.1 to 2.5 m. To conserve volume when thick floes combine or grow due to freezing, the fourteenth thickness category incorporates all thicknesses greater than 2.5 m. We examine the numerical convergence of the model in the Supplement (Sect. S2), finding that increasing this resolution does not significantly alter the numerical results.

The difference between the model state after a single 1 h time step and the model initial conditions is shown in Fig. 3b–d. Cooling leads to growth in both thickness and size (Fig. 3b) with the impact of lateral growth being less visible than the change in thickness. The shift in thickness is seen by the negative tendency (blue shading) for thicknesses smaller than the maximum of the initial distribution, and positive tendency at sizes larger than the initial maximum (red shading). These tendencies correspond to the shifting of floes from thinner to thicker floes due to the freezing. The shift in horizontal size is less apparent in the figure, due to the separation of scales between size and thickness; lateral growth rates are comparable to vertical growth rates ($1\,\mathrm{cm\,day^{-1}}$), but given that there is more than an order of magnitude difference between the floe size and thickness, the size change corresponds to a smaller relative change than the thicknesses change. The size response would be more apparent for smaller initial floe sizes not included in this idealized model experiment.

Mechanical interactions (Fig. 3c) lead to growth at three distinct clusters of size and thickness. The first, due to the self-interaction (rafting) of floes of size I, is shown as a positive tendency at a floe size of 123 m and thickness of 0.35 m. This cluster would not be resolved in a model that represented the ice thickness distribution only. The second cluster is due to a ridging interaction between floes of size I and II, leading to new floes of around 90 m size and 0.5 m thickness. The third, due to self-interaction (ridging) between floes of size II, leads to a positive tendency at floe sizes around 17 m and thickness around 1.7 m. Both the second and third clusters of floes would not be resolved in a model that represents the floe size distribution only, showing again the importance of representing the joint FSTD.

Swell fracture (Fig. 3d) leads to the fracturing of many of the floes of size I, shown as a negative tendency at the eliminated size class. Floes of size II are not affected because they are smaller than twice the wavelength of the specified surface gravity wave field. Since the specified wave field is monochromatic, the area of floes of size I that are broken is shown as a positive tendency at a floe size equal to half of the wavelength of the surface gravity wave, $\lambda / 2 = 28\,\mathrm{m}$. Ice thickness does not change when the ice is fractured.

Next, two 1-month simulations are performed using the same initial distribution to show the behavior of the model forced by two different fixed strain rate scenarios (Fig. 4). The first (Fig. 4a, b) simulates convergence of fixed magnitude ($\epsilon_{\mathrm{I}} = -10^{-7}, \epsilon_{\mathrm{II}} = 0)\,\mathrm{s^{-1}}$, and the second (Fig. 4c, d)

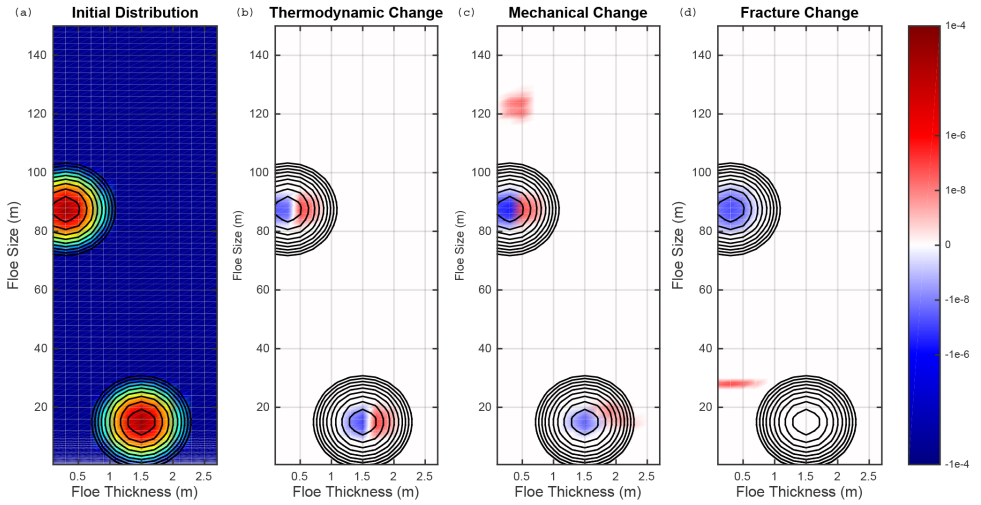

Figure 3. Response of the FSTD to idealized single-process experiments over a single time step (Sect. 3). **(b)** Change in response to thermodynamic forcing only. **(c)** Change in response to mechanical forcing only. **(d)** Change in response to wave forcing only. Solid black contours in **(b–d)** show the initial floe size and thickness distribution, and contour intervals are powers of 10. The color bar on the right corresponds to the change in the FSTD in units of fractional area per time step ($1\,s^{-1}$). Warm colors indicate an increase in fractional area, cool colors indicate a decrease in fractional area.

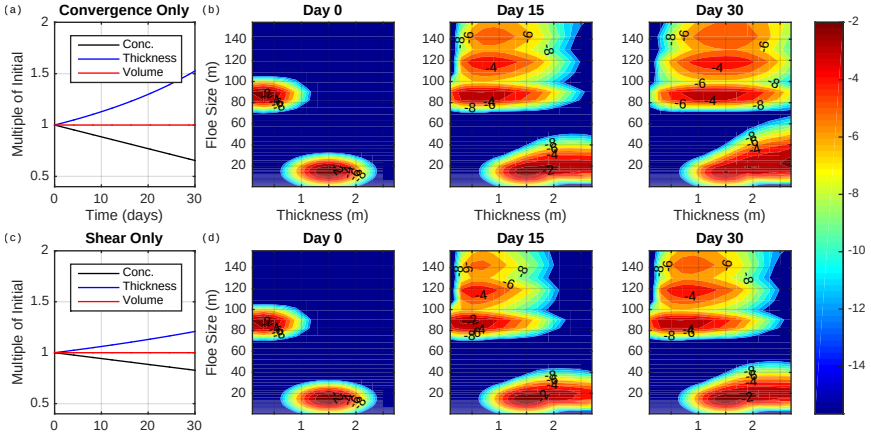

Figure 4. Results of two simulations of the floe size and thickness distribution forced with fixed ice-flow strain rates and only mechanical interactions. **(a)** Ice concentration, mean thickness, and ice volume for 1 month of fixed shear, with no convergence. Time series are normalized by their initial values. **(b)** The base 10 logarithm of the FSTD at days 0, 15, and 30 for the run with only shear. The color bar corresponds to the base 10 logarithm of the FSTD, contour intervals are powers of 10. **(c, d)** Same as **(a, b)** for 1 week of fixed convergence with no shear.

simulates shear of fixed magnitude ($\epsilon_{\mathrm{I}} = 0, \epsilon_{\mathrm{II}} = 10^{-7}$) s^{-1}. When there is no convergence, the rate of open water formation due to collisions (Eq. 13) is $0.5 \times 10^{-7}\,s^{-1}$, equal to the magnitude of the strain rate tensor divided by 2:

$$\left.\frac{D_{\mathrm{M}}c}{Dt}\right|_{\mathrm{shear}} = \frac{1}{2}\left(\epsilon_{\mathrm{I}} - ||\boldsymbol{E}||\right) = -\frac{1}{2}||\boldsymbol{E}||.$$

When there is no shear, and only convergence, the amount of open water formation due to collisions is $10^{-7}\,s^{-1}$, equal to the magnitude of the strain rate tensor:

$$\left.\frac{D_{\mathrm{M}}c}{Dt}\right|_{\mathrm{conv}} = \frac{1}{2}\left(\epsilon_{\mathrm{I}} - ||\boldsymbol{E}||\right) = -\frac{1}{2}\left(|\epsilon_I| + |\epsilon_I|\right) = -||\boldsymbol{E}||.$$

In both scenarios the norm of the strain rate tensor is the same, $||\boldsymbol{E}|| = 10^{-7}\,s^{-1}$. In the case of only shear (Fig. 4c,d), ice concentration is diminished by a factor of roughly 18 %, corresponding to a 22 % increase in mean ice thickness, and with no change in ice volume. In contrast, in the case of convergence only (Fig. 4a, b), ice concentration is diminished by 36 %, with a corresponding 56 % increase in mean ice thickness, again with no change in ice volume. Thus shear motions lead to collisions and the combinations of floes with one another, but at a reduced rate when compared to convergence of ice flow, for the same strain rate tensor norm. In the case of shear only, the two initial peaks in the FSTD are smeared

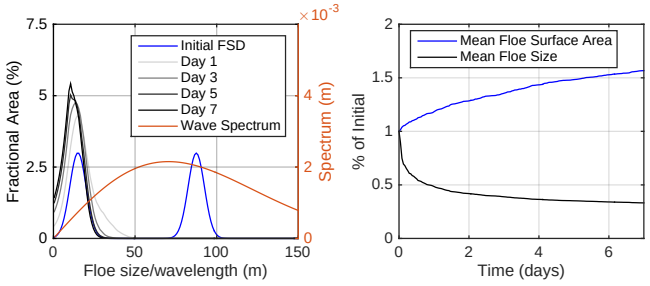

Figure 5. Results of simulations of the FSTD forced with swell fracture only. **(a)** The FSD before (black line, left axis) and after (gray lines, left axis) several days of swell fracture using a Bretschneider (Michel, 1968, p. 23) wave spectrum (orange line, right axis). As swell fracture does not affect floe thickness, the distribution is plotted as a function of floe size only. **(b)** The mean floe size and total lateral ice surface area as a fraction of their initial values over the course of 1 week of ice fracture with the specified wave spectrum.

out over a range of floe sizes and thicknesses (Fig. 4b), with the variety of floe sizes and thicknesses increasing in number over time. Since there is twice as much open water formation in the case of convergence only, and therefore an increased number of mechanical interactions, the distribution of floe sizes and thickness is smeared more rapidly, and over a larger range (Fig. 4c).

Figure 5 shows the response of the joint floe size and thickness distribution to a single-week experiment that simulates a 7-day period of ice fracture by surface waves, using a wave spectrum that leads to ice breaking into a broader range of floe sizes. The experiment uses the Bretschneider (Michel, 1968, p. 24) surface wave spectrum as a function of period T, $S(T)\,\mathrm{d}T$:

$$S(T)\,\mathrm{d}T = \frac{1 H_s^2}{4\pi T_z}\left(\frac{T}{T_z}\right)^3 e^{-\frac{1}{\pi}\left(\frac{T}{T_z}\right)^4}\mathrm{d}T,$$

where $H_s = 2\,\mathrm{m}$ is the significant wave height (the mean wave height of the 1/3 highest surface waves), and $T_z = 6\,\mathrm{s}$ is the mean time interval between zero-crossings of the observed wave record. We use the surface gravity wave dispersion relation $\lambda = gT^2/2\pi$ to write $S(T)\,\mathrm{d}T$ as a wavelength spectrum $S(\lambda)\,d\lambda$. The wavelength bins are spaced to correspond uniquely to floe size bins, and there is a one-to-one relationship between a wave's wavelength and the floe size of new floes formed through fracture of existing floes by that wave. The peak wavelength of the wave spectrum is at $T \approx 6.75\,\mathrm{s}$, corresponding to $\lambda \approx 70\,\mathrm{m}$. As before, the domain width D is set to 10 km. Large floes (size I) are rapidly fractured, with the fractional area corresponding to these floes decreasing, and the distribution shifts towards smaller sizes (Fig. 5a, gray lines). After 1 week, the fractional area belonging to floes in the range from 75 to 125 m decreases from 37 to 0 %, with mean floe size decreasing by 67 % (Fig. 5b, blue line). As a consequence, the total lateral surface area rises as floes are broken and their lateral sides are exposed, increasing by 63 % over the week (Fig. 5b, blue line).

4 Conclusions

We developed a model that simulates the evolution of the FSTD, using large-scale oceanic and atmospheric forcing fields as input, which may be useful as an extension to sea-ice models presently used in global climate models, in particular in regions with a continuously varying FSTD, such as the marginal ice zone. We included representations of the impact of thermodynamics (melting and freezing), mechanical interactions of rafting and ridging due to floe collisions, and of floe fracture by ocean surface waves, all processes that are active in marginal or seasonal sea-ice zones. We demonstrated the effect of these processes using model runs forced by external forcing fields including air–sea heat flux, ice flows leading to mechanical interactions, and specified surface wave field, and considered the effects of these forcing fields individually and when combined. We demonstrated the effects of mechanical interactions in the presence of both shearing and straining ice flows, separately accounting for ridging and rafting. We studied the effect of surface waves, first for idealized single-wavelength wave fields, and then accounting for a more realistic surface wave spectrum. We examined the response to melting and freezing both along existing floe bases and lateral edges, and in open water, leading to pancake ice formation.

While the present paper focuses on the development of parameterizations needed to represent the FSTD dynamics and to test the model with individual forcing fields, we hope to next study the consequences of realistic forcing fields on the FSTD and compare model output to the few available observations. Another important future direction is the model development and testing that will allow for implementation of this model into sea-ice models used in GCMs, allowing for realistic ice thermodynamics, constitutive stress–strain relationship, wave model, and ice motions driven by ocean currents and winds. At the same time, an implementation into a GCM would require making the model more efficient by replacing the high resolution we could afford to use here in floe size and thickness by a simplified approach, possibly assuming a functional form of the FSTD and simulating only its moments as is often done in atmospheric models of the particle size distribution.

The study of FSTD dynamics, and the development of a prognostic FSTD model, are made difficult by the scarcity of observations of the floe size distribution and its seasonal and long-term evolution. Such observations are required to constrain uncertain parameters used in the model developed here, and to help determine the dominant processes which need to be included in FSTD models to be incorporated in global climate models.

Appendix A: Comparison of rate constants in Eq. (14) to those in Thorndike et al. (1975)

Thorndike et al. (1975) employed the following parameterization of the function ψ (Eq. 1), which represents the rate of change of area belonging to ice of thickness h due to mechanical interactions:

$$\psi = \left(\epsilon_{\mathrm{I}}^2 + \epsilon_{\mathrm{II}}^2\right)^{1/2} \left(\alpha_0 \delta(h) + \alpha_{\mathrm{r}} w_{\mathrm{r}}(h)\right), \tag{A1}$$

where $\int_0^\infty w_{\mathrm{r}}(h) = -1$, and the coefficients α_0 and α_c are

$$\alpha_0 = \frac{1}{2}\left(1 + \cos(\theta)\right), \tag{A2}$$

$$\alpha_c = \frac{1}{2}\left(1 - cos(\theta)\right), \tag{A3}$$

where $\theta = \arctan(\epsilon_{\mathrm{II}} / \epsilon_I)$. Using the trigonometric identity,

$$\cos(\arctan(\epsilon_{\mathrm{II}} / \epsilon_I)) = \frac{\epsilon_I}{||E||},$$

with $||E|| \equiv \sqrt{\epsilon_{\mathrm{I}}^2 + \epsilon_{\mathrm{II}}^2}$, ψ may be rewritten as

$$\psi = \frac{1}{2}||E|| \left(\delta(h)\frac{||E|| + \epsilon_I}{||E||} + \frac{||E|| - \epsilon_I}{||E||} w_r\right), \tag{A4}$$

$$= \frac{1}{2}\left(\delta(h)(||E|| + \epsilon_{\mathrm{I}}) + w_{\mathrm{r}}(||E|| - \epsilon_{\mathrm{I}})\right), \tag{A5}$$

$$= \delta(h)\epsilon_{\mathrm{I}} + \frac{1}{2}\left(||E|| - \epsilon_{\mathrm{I}}\right)\left(\delta(h) + w_{\mathrm{r}}\right). \tag{A6}$$

Identifying $w_r = -\int_{\mathrm{h}} L_{\mathrm{c}}(\boldsymbol{r})\,\mathrm{d}h$ and $\frac{1}{2}\left(||E|| - \epsilon_{\mathrm{I}}\right) = \frac{D_{\mathrm{M}c}}{Dt}$ recovers the floe-size-integrated form of Eq. (14).

The Supplement related to this article is available online at doi:10.5194/tc-9-2119-2015-supplement.

Acknowledgements. We thank Luke Bennetts and an anonymous reviewer for their most detailed, constructive, knowledgeable, and helpful comments. This research was supported by NASA under grant NNX14AH39G. C. Horvat was supported by the Department of Defense (DoD) through the National Defense Science & Engineering Graduate Fellowship (NDSEG) Program. E. Tziperman thanks the Weizmann Institute for its hospitality during parts of this work.

Edited by: D. Feltham

References

Asplin, M. G., Galley, R., Barber, D. G., and Prinsenberg, S.: Fracture of summer perennial sea ice by ocean swell as a result of Arctic storms, J. Geophys. Res., 117, 1–12, doi:10.1029/2011JC007221, 2012.

Asplin, M. G., Scharien, R., Else, B., Howell, S., Barber, D. G., Papakyriakou, T., and Prinsenberg, S.: Implications of fractured Arctic perennial ice cover on thermodynamic and dynamic sea ice processes, J. Geophys. Res. Oceans, 119, 2327–2343, doi:10.1002/2013JC009557, 2014.

Bennetts, L. G. and Squire, V. A.: Model sensitivity analysis of scattering-induced attenuation of ice-coupled waves, Ocean Model., 45–46, 1–13, doi:10.1016/j.ocemod.2012.01.002, 2012.

Bennetts, L. G. and Williams, T. D.: Water wave transmission by an array of floating disks, Proc. Roy. Soc. A, 471, 1–18, doi:10.1098/rspa.2014.0698, 2015.

Birnbaum, G. and Lüpkes, C.: A new parameterization of surface drag in the marginal sea ice zone, Tellus A, 54, 107–123, doi:10.1034/j.1600-0870.2002.00243.x, 2002.

Bitz, C. M.: Numerical modeling of sea ice in the climate system, Tech. rep., University of Washington, www.atmos.uw.edu/~bitz/Bitz_chapter.pdf (last access: 11 October 2015), 2008.

Bitz, C. M., Holland, M. M., Weaver, A. J., and Eby, M.: Simulating the ice-thickness distribution in a coupled climate model, J. Geophys. Res., 106, 2441, doi:10.1029/1999JC000113, 2001.

Bourke, R. H. and Garrett, R. P.: Sea ice thickness distribution in the Arctic Ocean, Cold Reg. Sci. Technol., 13, 259–280, doi:10.1016/0165-232X(87)90007-3, 1987.

Bouws, E., Draper, L., Shearman, E., Laing, A., Feit, D., Mass, W., Eide, L., Francis, P., Carter, D., and Battjes, J.: Guide to Wave analysis and forecasting, World Meteorological Organization, 1998, 11–12, 1998.

Cavalieri, D. J. and Parkinson, C. L.: Arctic sea ice variability and trends, 1979–2010, The Cryosphere, 6, 881–889, doi:10.5194/tc-6-881-2012, 2012.

Chevallier, M. and Salas-Mélia, D.: The role of sea ice thickness distribution in the arctic sea ice potential predictability: A diagnostic approach with a coupled GCM, J. Clim., 25, 3025–3038, doi:10.1175/JCLI-D-11-00209.1, 2012.

Collins, C. O., Rogers, W. E., Marchenko, A., and Babanin, A. V.: In situ measurements of an energetic wave event in the Arctic marginal ice zone, Geophys. Res. Lett., 42, 1863–1870, doi:10.1002/2015GL063063, 2015.

Dumont, D., Kohout, A., and Bertino, L.: A wave-based model for the marginal ice zone including a floe breaking parameterization, J. Geophys. Res., 116, C04001, doi:10.1029/2010JC006682, 2011.

Feltham, D. L.: Granular flow in the marginal ice zone., Phil. T., 363, 1677–1700, doi:10.1098/rsta.2005.1601, 2005.

Feltham, D. L.: Sea Ice Rheology, Ann. Rev. Fluid Mech., 40, 91–112, doi:10.1146/annurev.fluid.40.111406.102151, 2008.

Godlovitch, D., Illner, R., and Monahan, A.: Smoluchowski coagulation models of sea ice thickness distribution dynamics, J. Geophys. Res., 116, C12005, doi:10.1029/2011JC007125, 2011.

Harvey, L. D. D.: Testing alternative parameterizations of lateral melting and upward basal heat flux in a thermodynamic sea ice model, J. Geophys. Res., 95, 7359, doi:10.1029/JC095iC05p07359, 1990.

Henderson, G. R., Barrett, B. S., and Lafleur, D.: Arctic sea ice and the Madden-Julian Oscillation (MJO), Clim. Dynam., 43, 2185–2196, doi:10.1007/s00382-013-2043-y, 2014.

Herman, A.: Sea-ice floe-size distribution in the context of spontaneous scaling emergence in stochastic systems, Phys. Rev. E., 81, 066123, doi:10.1103/PhysRevE.81.066123, 2010.

Herman, A.: Molecular-dynamics simulation of clustering processes in sea-ice floes, Phys. Rev. E, 1–25, 2011.

Herman, A.: Numerical modeling of force and contact networks in fragmented sea ice, Ann. Glaciol., 54, 114–120, doi:10.3189/2013AoG62A055, 2013.

Hibler, W. D.: A Dynamic Thermodynamic Sea Ice Model, J. Phys. Oceanogr., 9, 815–846, doi:10.1175/1520-0485(1979)009<0815:ADTSIM>2.0.CO;2, 1979.

Hibler III, W. D.: Modeling a variable thickness ice cover, Mon. Weather Rev., 108, 1943–1973, 1980.

Holt, B. and Martin, S.: The effect of a storm on the 1992 summer sea ice cover of the Beaufort, Chukchi, and East Siberian Seas, J. Geophys. Res., 106, 1017, doi:10.1029/1999JC000110, 2001.

Hopkins, M. A., Tuhkuri, J., and Lensu, M.: Rafting and ridging of thin ice sheets, J. Geophys. Res., 104, 13605, doi:10.1029/1999JC900031, 1999.

Horvat, C. and Tziperman, E.: Effects of the Sea Ice Floe Size Distribution on Polar Ocean Properties and Air-Sea Exchange, in: Abstract C11A-0341 presented at 2014 Fall Meeting, AGU, San Francisco, CA, 15–19 December, 2014.

Hunke, E. C., Lipscomb, W. H., Turner, A. K., Jeffery, N., and Elliot, S.: CICE: The Los Alamos Sea Ice Model Documentation and SoftwareUsers Manual Version 5.0, Tech. rep., Los Alamos Natl. Laboratory, Los Alamos, NM, 2013.

Johannessen, J. A., Johannessen, O. M., Svendsen, E., Shuchman, R., Manley, T., Campbell, W. J., Josberger, E. G., Sandven, S., Gascard, J. C., Olaussen, T., Davidson, K., and Van Leer, J.: Mesoscale eddies in the Fram Strait marginal ice zone during the 1983 and 1984 Marginal Ice Zone Experiments, J. Geophys. Res., 92, 6754, doi:10.1029/JC092iC07p06754, 1987.

Kohout, A. L., Williams, M., Toyota, T., Lieser, J., and Hutchings, J.: In situ observations of wave-induced sea ice breakup, Deep Sea Res., 1–6, doi:10.1016/j.dsr2.2015.06.010, 2015.

Kohout, A. L. and Meylan, M. H.: An elastic plate model for wave attenuation and ice floe breaking in the marginal ice zone, J. Geophys. Res., 113, C09016, doi:10.1029/2007JC004434, 2008.

Lu, P., Li, Z. J., Zhang, Z. H., and Dong, X. L.: Aerial observations of floe size distribution in the marginal ice zone of summer Prydz Bay, J. Geophys. Res., 113, C02011, doi:10.1029/2006JC003965, 2008.

McPhee, M. G.: Turbulent heat flux in the upper ocean under sea ice, J. Geophys. Res., 97, 5365, doi:10.1029/92JC00239, 1992.

Meylan, M. H., Bennetts, L. G., and A. L. Kohout: In situ measurements and analysis of ocean waves in the Antarctic marginal ice zone, Geophys. Res. Lett., 41, 1–6, doi:10.1002/2014GL060809.In, 2014.

Michel, W.: Sea Spectra Simplified, Marine Technol., 5, 17–30, 1968.

Niebauer, H.: Wind and melt driven circulation in a marginal sea ice edge frontal system: a numerical model, Cont. Shelf Res., 1, 49–98, doi:10.1016/0278-4343(82)90032-2, 1982.

Parkinson, C. L. and Washington, W. M.: A large-scale numerical model of sea ice, J. Geophys. Res., 84, 311–337, doi:10.1029/JC084iC01p00311, 1979.

Parmerter, R. R.: A model of simple rafting in sea ice, J. Geophys. Res., 80, 1948, doi:10.1029/JC080i015p01948, 1975.

Parmerter, R. R. and Coon, M. D.: Model of pressure ridge formation in sea ice, J. Geophys. Res., 77, 6565, doi:10.1029/JC077i033p06565, 1972.

Perovich, D. K. and Jones, K. F.: The seasonal evolution of sea ice floe size distribution, J. Geophys. Res.-Ocean., 119, 8767–8777, doi:10.1002/2014JC010136, 2014.

Renner, A. and Gerland, S.: Evidence of Arctic sea ice thinning from direct observations, Geophys. Res. Lett., 2012, 5029–5036, doi:10.1002/2014GL060369.1., 2014.

Rothrock, D. A. and Thorndike, A. S.: Measuring the sea ice floe size distribution, J. Geophys. Res., 89, 6477–6486, doi:10.1029/JC089iC04p06477, 1984.

Semtner, A. J.: A Model for the Thermodynamic Growth of Sea Ice in Numerical Investigations of Climate, J. Phys. Oceanogr., 6, 379–389, doi:10.1175/1520-0485(1976)006<0379:AMFTTG>2.0.CO;2, 1976.

Shen, H., Hibler, W., and Leppäranta, M.: On applying granular flow theory to a deforming broken ice field, Acta Mech., 143–160, doi:10.1007/BF01182545, 1986.

Shen, H. H. and Sankaran, B.: Internal Length And Time Scales In A Simple Shear Granular Flow, Phys. Rev. E, 70, 51308, doi:10.1103/PhysRevE.70.051308, 2004.

Shen, H. H., Hibler, W. D., and Leppäranta, M.: The role of floe collisions in sea ice rheology, J. Geophys. Res., 92, 7085, doi:10.1029/JC092iC07p07085, 1987.

Steele, M.: Sea ice melting and floe geometry in a simple ice-ocean model, J. Geophys. Res., 97, 17729, doi:10.1029/92JC01755, 1992.

Steer, A., Worby, A., and Heil, P.: Observed changes in sea-ice floe size distribution during early summer in the western Weddell Sea, Deep-Sea Res. II, 55, 933–942, doi:10.1016/j.dsr2.2007.12.016, 2008.

Stroeve, J. C., Serreze, M. C., Holland, M. M., Kay, J. E., Malanik, J., and Barrett, A. P.: The Arctic's rapidly shrinking sea ice cover: A research synthesis, Clim. Change, 110, 1005–1027, doi:10.1007/s10584-011-0101-1, 2012.

Strong, C. and Rigor, I. G.: Arctic marginal ice zone trending wider in summer and narrower in winter, Geophys. Res. Lett., 40, 4864–4868, doi:10.1002/grl.50928, 2013.

Strong, C., Magnusdottir, G., and Stern, H.: Observed feedback between winter sea ice and the North Atlantic Oscillation, J. Clim., 22, 6021–6032, doi:10.1175/2009JCLI3100.1, 2009.

Thorndike, A. S., Rothrock, D. A., Maykut, G. A., and Colony, R.: The thickness distribution of sea ice, J. Geophys. Res., 80, 4501, doi:10.1029/JC080i033p04501, 1975.

Toyota, T. and Enomoto, H.: Analysis of sea ice floes in the Sea of Okhotsk using ADEOS/AVNIR images, in: Proceedings of the 16th IAHR International Symposium on Ice, 211–217, International Association of Hydraulic Engineering and Research, 2002.

Toyota, T., Takatsuji, S., and Nakayama, M.: Characteristics of sea ice floe size distribution in the seasonal ice zone, Geophys. Res. Lett., 33, L02616, doi:10.1029/2005GL024556, 2006.

Toyota, T., Haas, C., and Tamura, T.: Size distribution and shape properties of relatively small sea-ice floes in the Antarctic marginal ice zone in late winter, Deep-Sea Res. II, 58, 1182–1193, doi:10.1016/j.dsr2.2010.10.034, 2011.

Vavrus, S. J., Holland, M. M., Jahn, A., Bailey, D. A., and Blazey, B. A.: Twenty-first-century arctic climate change in CCSM4, J. Clim., 25, 2696–2710, doi:10.1175/JCLI-D-11-00220.1, 2012.

Washington, W. M., Semtner, A. J., Parkinson, C., and Morrison, L.: On the Development of a Seasonal Change Sea-Ice Model, J. Phys. Oceanogr., 6, 679–685, doi:10.1175/1520-0485(1976)006<0679:OTDOAS>2.0.CO;2, 1976.

Williams, T. D., Bennetts, L. G., Squire, V. a., Dumont, D., and Bertino, L.: Wave–ice interactions in the marginal ice zone. Part 1: Theoretical foundations, Ocean Model., 71, 81–91, doi:10.1016/j.ocemod.2013.05.010, 2013a.

Williams, T. D., Bennetts, L. G., Squire, V. A., Dumont, D., and Bertino, L.: Wave-ice interactions in the marginal ice zone. Part 2: Numerical implementation and sensitivity studies along 1D transects of the ocean surface, Ocean Model., 71, 92–101, doi:10.1016/j.ocemod.2013.05.011, 2013b.

Wu, Q. and Zhang, X.: Observed evidence of an impact of the Antarctic sea ice dipole on the Antarctic oscillation, J. Clim., 24, 4508–4518, doi:10.1175/2011JCLI3965.1, 2011.

Yu, Y. and Rothrock, D. A.: Thin ice thickness from satellite thermal imagery, J. Geophys. Res., 101, 25753, doi:10.1029/96JC02242, 1996.

Zhang, J., Lindsay, R., Schweiger, A., and Steele, M.: The impact of an intense summer cyclone on 2012 Arctic sea ice retreat, Geophys. Res. Lett., 40, 720–726, doi:10.1002/grl.50190, 2013.

Zhang, J., Schweiger, A., Steele, M., and Stern, H.: Sea ice floe size distribution in the marginal ice zone: Theory and numerical experiments, J. Geophys. Res.-Ocean., 120, 3484—-3498, doi:10.1002/2015JC010770, 2015.

Supplement of The Cryosphere, 9, 2119–2134, 2015
http://www.the-cryosphere.net/9/2119/2015/
doi:10.5194/tc-9-2119-2015-supplement

The Cryosphere Open Access EGU

Supplement of

A prognostic model of the sea-ice floe size and thickness distribution

C. Horvat and E. Tziperman

Correspondence to: C. Horvat (horvat@fas.harvard.edu)

A prognostic model of the sea ice floe size and thickness distribution

Christopher Horvat and Eli Tziperman

School of Engineering and Applied Sciences and Department of Earth and Planetary Sciences, Harvard University

Supplementary Materials

Contents

S1 Sensitivity tests

We examine the sensitivity of model results to perturbations in the set of parameters listed, along with sensitivity ranges, in Table S1, The perturbed parameters represent each of the model components. These tests demonstrate the robustness of the model to changes in the main model parameters, at the same time indicating the need to further constrain the relevant parameters.

S1.1 Thermodynamics

Model parameters that govern the thermodynamic model component include the pancake floe size $r_{\min}$, pancake floe thickness $h_{\min}$, and width of the lead region, r_{lw}. To examine the model sensitivity to changes in these parameter values, the model is initialized with zero ice concentration, with only the thermodynamic component of the model enabled. The external forcing is a net cooling heat flux $Q_{ex} = -50\mathrm{W/m}^2$, of which a proportion equal to $(1-c)Q_{ex}$, where c is the ice concentration, is applied to water (assumed to be at its freezing temperature). This cooling over water is further decomposed into an "open water" cooling of magnitude Q_o, which leads to the growth of ice pancakes, and a "lead" cooling of magnitude Q_l that leads to lateral and basal freezing, as outlined in the manuscript (Sec. 2.1). The net cooling in the region covered by ice has magnitude cQ_{ex}, and leads to only lateral and basal freezing, not to the formation of ice pancakes. To maintain a fixed grid in size and thickness space across all experiments, the pancake floe size

Parameter	Description	component	Range
$r_{\min}$	Pancake floe size	thermo	1 m $\pm$ 0.5 m
r_{lw}	Lead region width	thermo	1 m $\pm$ 0.5 m
$h_{\min}$	Pancake floe thickness	thermo	0.2 m $\pm$ 0.1 m
δ_{ridge}	Ridge width	mechanics	5 m $\pm$ 2.5 m
k_{ridge}	Ridging thickness mult.	mechanics	5 $\pm$ 2
v_{g}	Wave-ice group velocity	waves	$(1 \pm \frac{1}{2}) \cdot \frac{1}{2}\sqrt{\mathrm{g/k}}$ m/s
ϵ_{crit}	Crit. failure threshold	waves	$5 \cdot 10^{-6}$ - $5 \cdot 10^{-5}$ 1/s
α	Attenuation Coefficient	waves	KM08 or BS12

Table S1: Parameters varied in sensitivity tests, with the range of values used in sensitivity tests

and thickness are specified separately from the smallest resolved floe size and thickness, which is held constant in these runs, equal to 0.5 m and 0.1 m, respectively. Each run has an evenly spaced grid of 400 floe sizes from 0.5 m to 200 m, and 14 floe thicknesses from 0.1 m to 2.7 m.

First, the pancake ice thickness, $h_{\min}$, is varied from 0.1 m to 0.3 m. Fig. S1 shows the model response in terms of the total ice volume (Fig. S1a), ice concentration (Fig. S1b) and open water cooling Q_o (Fig. S1c). All runs have the same ice volume over time, since the net cooling is fixed. When the specified pancake thickness is larger, the added area of pancakes formed by the same net cooling must decrease, as volume is conserved. Accordingly, after 15 days the ice concentration in the experiment where $h_{\min} = .3$ m is 45% of that in the experiment where $h_{\min} = .1$ m.

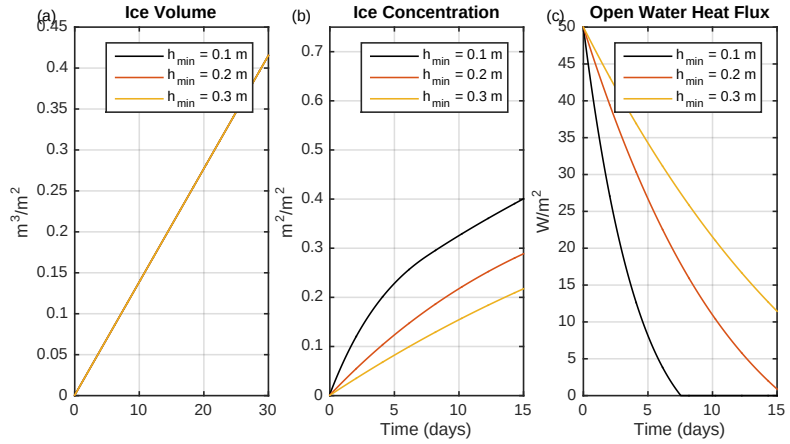

Figure S1: Sensitivity to the variation of the pancake ice thickness $h_{\min}$ from 0.1 m to 0.3 m, for an initially uncovered sea surface with a net applied cooling of 50W/m^2. (a) Ice volume, (b) ice concentration, and (c) net heat flux to the open water region for each run. Black lines correspond to default model values, $h_{\min} = 0.1$ m.

We next separately vary the lateral size of ice pancakes, $r_{\min}$, and the width of the lead region, r_{lw}, from 0.5 m to 1.5 m (Fig. S2). The ice volume is the same across both sets of runs (Fig. S2a,d), since the net cooling is fixed. First, we perturb $r_{\min}$ (Fig. S2 a-c). Since a portion of the cooling in the lead region contributes to the vertical growth of existing floes, cooling in the open water region leads to higher rates of ice concentration growth.

Thus, decreasing the size of the lead region leads to an increase in the rate of increase of ice concentration. Increasing the pancake floe size leads to an increase in the net open water heat flux, and therefore a more rapid increase in the ice concentration (Fig. S2b,c). After 15 days, ice concentration increases by 35% between the run in which $r_{\min} = 0.5$ m and the run in which $r_{\min} = 1.5$ m. In the second set of experiments, r_{lw} varies from 0.5 m to 1.5 m (Fig. S2d-f). Increasing the width of leads decreases the size of the open water region (Fig. S2f), leading to a slower increase in ice concentration. After 15 days, ice concentration decreases by 43% as r_{lw} increases by 200% (Fig. S2e).

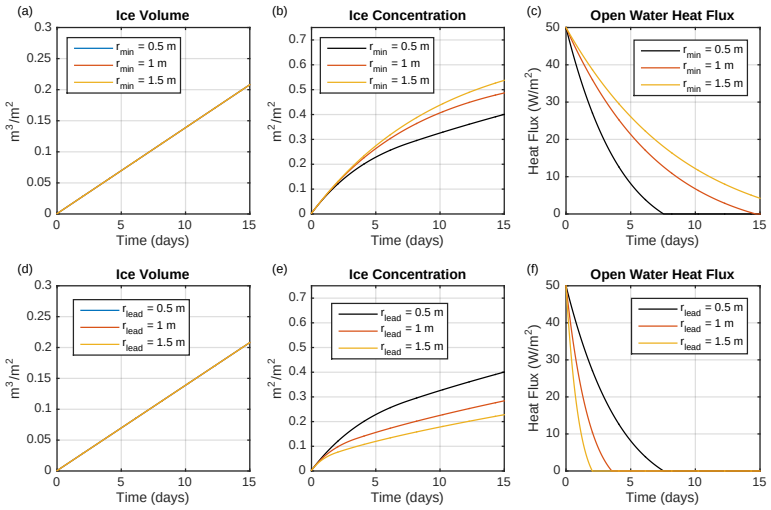

Figure S2: Sensitivity to the variation of the lead width r_{lw} and minimum floe size $r_{\min}$, for an initially uncovered sea surface with a net applied cooling of $50\mathrm{W/m}^2$. (a) Ice volume, (b) ice concentration, and (c) open water heat flux, for runs in which $r_{\min}$ is varied from 0.5 m to 1.5 m. (d-f) Same as (a-c), but when r_{lw} is varied from 0.5 m to 1.5 m. Black lines correspond to default model values, $r_{lw} = r_{\min} = 0.5$ m.

S1.2 Mechanics

This set of runs is initialized as in Sec. 3 of the manuscript, with two Gaussian peaks in the FSTD. The first peak has a mean size of 90 m and a mean

thickness of 0.25 m. The second peak has a mean size of 15 m and a mean thickness of 1.5 m, and only the mechanical component of the model is enabled. The external forcing is defined to be a set convergence of 1×10^7 1/s, applied for 30 days. These model runs are performed using the original floe size discretization outlined in the manuscript, spaced according to $r_{n+1} = \sqrt{6/5} r_n$, $r_1 = 0.5$ m, with 64 bins up to 156 m. Each run has an evenly spaced grid of 14 floe thicknesses from 0.1 m to 2.7 m.

Parameters that influence the mechanical component of the FSTD model are the widths ($\delta_{\text{ridge/raft}}$) of ridges and rafts formed in floe collisions, and the thickness multiple k_{ridge}, the ratio of the thickness of a new ridge to the thickness of the smallest of two combining floes. Since we represent rafting and ridging similarly in the model, we examine only sensitivity to ridging parameters. The ridge width is varied from 3 to 7 meters, and the ridging thickness multiple is varied from 3 to 7. The response is seen in Fig. S3, note that the vertical scale is logarithmic.

The influence of changing the ridging multiple is minor, with little impact on either the FSD or ITD after 30 days (Fig. S3a,c). Changing the ridge width (Fig. S3b,d) influences the spread of smaller floes to larger sizes, and increasing the ridge width leads to more floes at smaller sizes, though the major differences are seen at sizes and thicknesses with concentration less than 1%, so the model results are largely insensitive to these parameters.

S1.3 Wave-induced fracture

This set of runs is initialized with a single Gaussian peak in the floe size distribution at 90 m size and 1 m thickness. The fracture component of the FSTD model is turned on, and all other model components are turned off. The model discretization is the same as in Sec. S1.2. The external forcing consists of a Bretschneider surface wave spectrum, with a zero-crossing period of 6 s and a significant height of 2 m, and is continuously applied for seven days at the ice edge. The model domain width is 10km.

Model parameters that influence the response of the FSTD to fracture of ice by ocean surface waves are the group velocity of waves in ice, v_{g} and the flexural strain failure threshold ϵ_{crit}. The wave group velocity is varied from 0.5 to 1.5 times the surface gravity wave group velocity. The failure threshold is varied over an order of magnitude from $5{\times}10^{-6}$ 1/s to $5.5{\times}10^{-5}$ 1/s. The response to the variation of these two parameters is shown in Fig. S4.

The group velocity changes the fraction of the model domain affected by

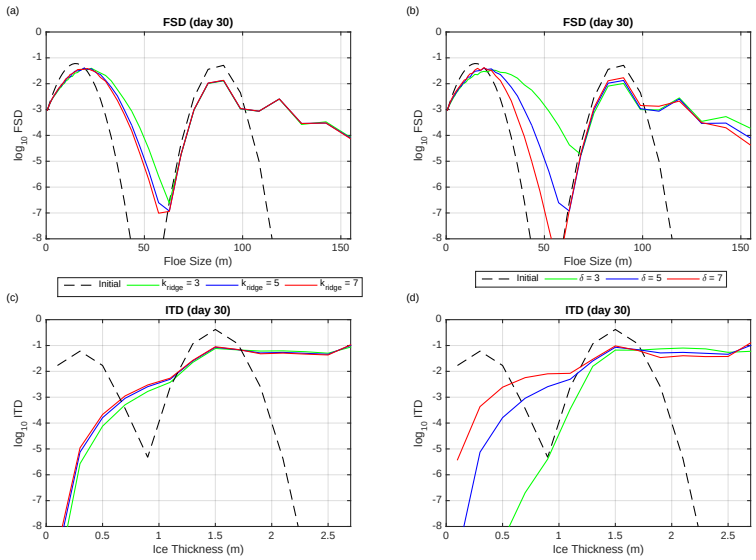

Figure S3: Sensitivity to the variation of ridge width and thickness multiple for the mechanical sensitivity run. (a,c) Base 10 log of the FSD (a) and ITD (c) after 30 days, when the ridging thickness multiple is changed from 3 to 7. Dashed black line is the initial condition. (b,d) Base 10 log of the FSD (b) and ITD (d) after 30 days, when the width of ridges is changed from 3 m to 7 m

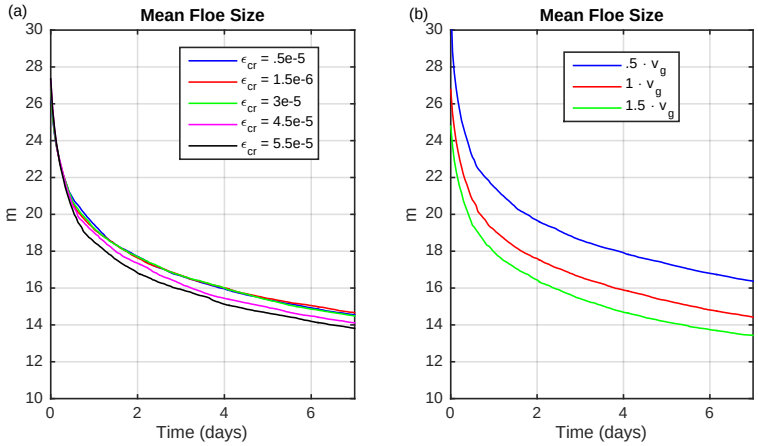

Figure S4: Sensitivity to the variation of parameters for runs with wave-induced fracture only, with a single Gaussian peak in the FSTD and 7 days of wave forcing. (a) Sensitivity of mean floe size to changes in ϵ_{crit}. (b) Sensitivity of mean floe size to the wave group velocity v_{g}.

fracturing and therefore the time-scale of breaking. There is limited sensitivity to changes in the critical strain coefficient, as strains calculated are on the order of 10^{-2} and higher (Fig.'S4a), suggesting that further study of the critical strain necessary to break floes by waves is necessary. As the wave group velocity is increased, more fracture occurs and the mean floe size decreases (Fig. S4b).

S1.4 Attenuation model

Additionally, the parameterization of wave attenuation influences the response of the FSTD to the fracture of ice by ocean waves. We perform the same runs as in Sec. S2.2, comparing the wave attenuation model outlined in Bennetts and Squire (2012) (hereafter BS12) to the one-dimensional scattering attenuation model that is outlined and implemented in the main paper (Kohout and Meylan, 2008, herafter KM08). A comparison of the attenuation coefficient used as input in our FSTD model, as a function of wave period and ice thickness, is shown in Fig. S5 (compare with Fig. 1 in the main paper).

Fig. S6 shows how the mean floe size differs between the two simulations. The results from the run using BS12 (blue lines) have a mean floe size that

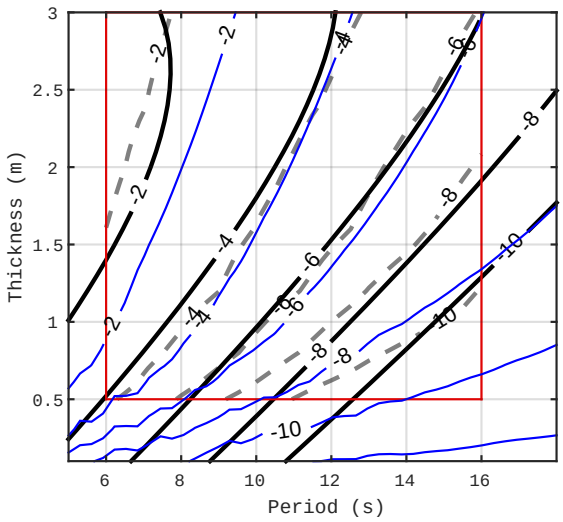

Figure S5: The natural logarithm of the attenuation coefficient α calculated by Kohout and Meylan (2008) (dash, inside the red box) and a quadratic fit to this attenuation coefficient that is used in section 4 of the manuscript (solid). Blue lines are the natural logarithm of the attenuation coefficient α as calculated by Bennetts and Squire (2012) and are not extrapolated. Solid contours outside of the red box are extrapolated using a quadratic fit. The fit is given by $\ln \alpha(T, \bar{h}) = -0.3203 + 2.058\bar{h} - 0.9375T - 0.4269\bar{h}^2 + 0.1566\bar{h}T + 0.0006T^2$.

is larger after one week than KM08 (red lines). The model results depend on the differences between the two parameterizations.

S2 Numerical convergence tests

To test for numerical convergence with respect to resolution in floe-size space, we examine two single-process runs (mechanics and wave-induced fracture), which are described below. The model runs are first performed using the original resolution used in the manuscript, spaced according to $r_{n+1} = \sqrt{6/5}r_n$, $r_1 = 0.5$ m, with 64 bins up to 156 m. A second set of model runs is

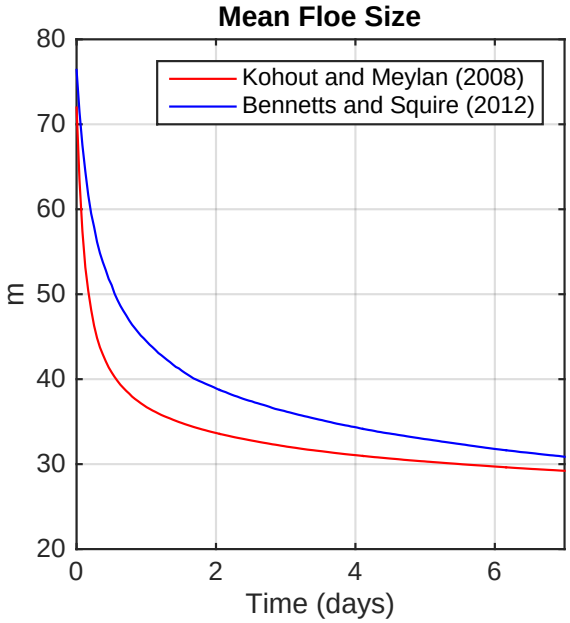

Figure S6: Comparison of the mean floe size in two week-long wave-induced fracture runs, using (red) the Kohout and Meylan (2008) or (blue) the Bennetts and Squire (2012) attenuation coefficient model. Both runs are initialized with a mean floe size of 87.5 m, the first time plotted here is the first model time step, one hour after the initialization.

performed using a doubled resolution, with 63 additional floe sizes spaced evenly between gridpoints of the original grid. These tests demonstrate the robustness of the model to changes in the grid resolution.

S2.1 Mechanics run

The initialization is as described in section S1.2. The mechanical interaction component of the model is turned on, while all other model components are turned off, with the results of this run shown in Fig. S7. The base 10

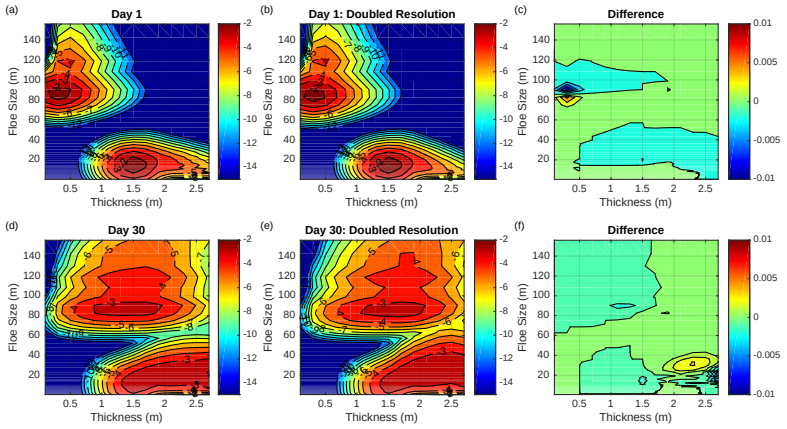

Figure S7: Base 10 logarithm of the FSTD for a regular resolution run (a,d) and doubled-resolution run (b,e) after 1 day (a-c) and 30 days (d-f). Contours are powers of ten in the distribution. (c,f) The difference (linear scale) between (a) and (b), and (d) and (e) when the doubled-resolution run is binned at the lower resolution.

logarithm of the FSTD after 1 day (Fig. S7a,d) and 30 days (Fig. S7b,e) are qualitatively similar. The difference between the two is calculated by binning the higher resolution into the lower resolution, and shows little difference between the two runs (Fig. S7c,f). The difference is nowhere larger than 1% in concentration after 30 days, so we conclude there is a limited sensitivity to resolution in these runs.

S2.2 Wave-induced fracture run

The initialization used is as described in section S1.3, and the results are seen in Fig. S8. Fig. S8a shows the base 10 logarithm of the FSD over

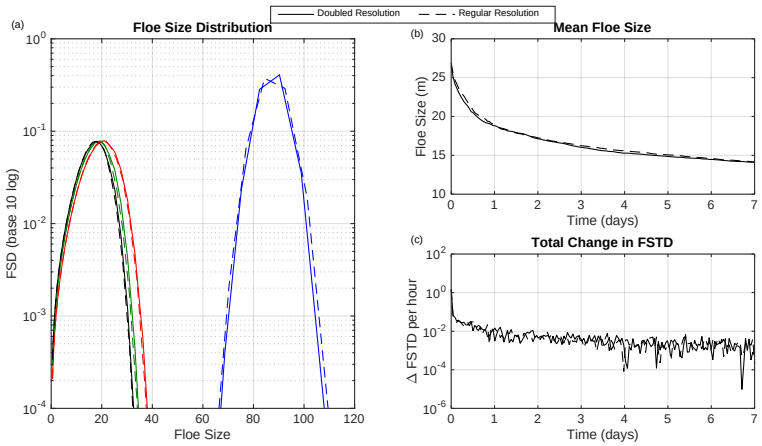

Figure S8: (a) Base 10 logarithm of the FSD for a regular resolution run (solid lines) and doubled-resolution run (dashed lines) at days 0 (blue), 2 (red), 4 (green) and 6 (black) of model runs that test convergence using wave-induced fracture alone. (b) The mean floe size over time for these runs. (c) The total fraction of the ice that is fractured, per day, for these runs.

time for the original (solid lines) and doubled (dashed lines) resolution runs, showing limited sensitivity to the shift in resolution. This is confirmed when examining the mean floe size (Fig. S8b), and additionally when examining the total area fractured per day (Fig. S8c), both of which are similar. We again conclude there is limited sensitivity to resolution in these runs.

S3 Calculation of Fractured Floe Size Distribution

We now demonstrate the wave fracture formulation with a specific example based on the Bretschneider wave spectrum $S_B(\lambda)$,

$$S_B(\lambda) = \frac{H_s^2}{8\pi}\frac{\lambda}{\lambda_z^2}e^{-\frac{1}{\pi}(\frac{\lambda}{\lambda_z})^2},$$

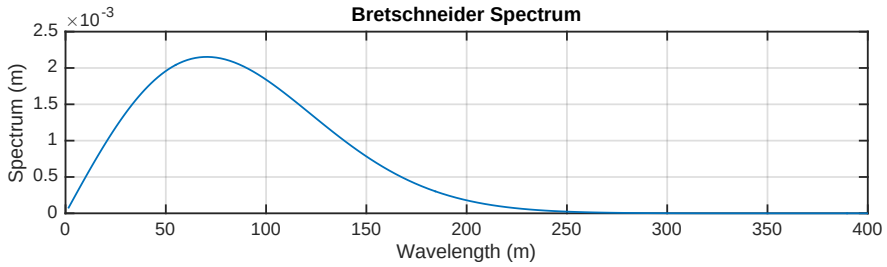

Figure S9: The Bretschneider wave spectrum $S_B(\lambda)$ (units of m) as a function of wavelength λ, for a significant wave height of 2m and zero-crossing period of 6s.

shown in Figure S9, with units of m, as a function of wavelength λ. The zero-crossing period T_z is 6s and significant wave height H_s is 2m. The parameter $\lambda_z = gT_z^2/2\pi$ is the mean zero-crossing wavelength, $\lambda_z \approx 55$ m. Using minimum and maximum wavelengths of $\lambda_{min} = .25$ m, $\lambda_{max} = 200$ m, and $\Delta\lambda = 0.25$ m, spectral amplitudes are defined as $a_i = \sqrt{2S_B(\lambda_i)\Delta\lambda}$, so that $\int S_B(\lambda)d\lambda \approx \sum_{i=1}^{N_\lambda} S_B(\lambda)\Delta\lambda = \sum_{i=1}^{N_\lambda} a_i^2/2$. The domain size is $D = 10$km, and $x = 0$ corresponds to the boundary from which waves enter the domain. There are $N_\lambda = \lambda_{max}/\Delta\lambda = 800$ spectral lines, and a realization of the sea surface height $\eta(x)$ is generated according to,

$$\eta(x_j) = \sum_{i=1}^{N_\lambda} a_i e^{-\alpha(\lambda_i)x_j} \cos\left(\frac{2\pi x_j}{\lambda_i} + \phi_i\right), \tag{1}$$

where $\alpha(\lambda_i)$ is the attenuation coefficient for waves of wavelength λ_i, and the random phases ϕ_i are drawn from a uniform distribution between 0 and 2π. The first 100 m of a sample generated $\eta(t)$ is plotted as Fig. S10 (blue line). We assume that the floe conforms to the sea surface, and that it will fracture when it is strained between three successive local extrema of η (Fig. S10, circles), where points are defined to be extrema when they are a local maximum or minimum over a distance of 10 m on each side. For a triplet of successive extrema (max, min, max; or min, max, min) of η, $(x_{i-1}^*, x_i^*, x_i^*)$, the strain felt by the floe at x_i^* is calculated by the finite difference approximation,

$$\epsilon(x_i^*) = \frac{h}{2}\frac{\partial^2\eta}{\partial x^2} \approx \frac{h}{2}\frac{\eta(x_{i-1}^*)\Delta x_{i+1}^* - \eta(x_i^*)(\Delta x_{i+1}^* + \Delta x_i^*) + \eta(x_i^*)\Delta x_i^*}{\Delta x_i^*\Delta x_{i+1}^*(\Delta x_i^* + \Delta x_{i+1}^*)}, \tag{2}$$

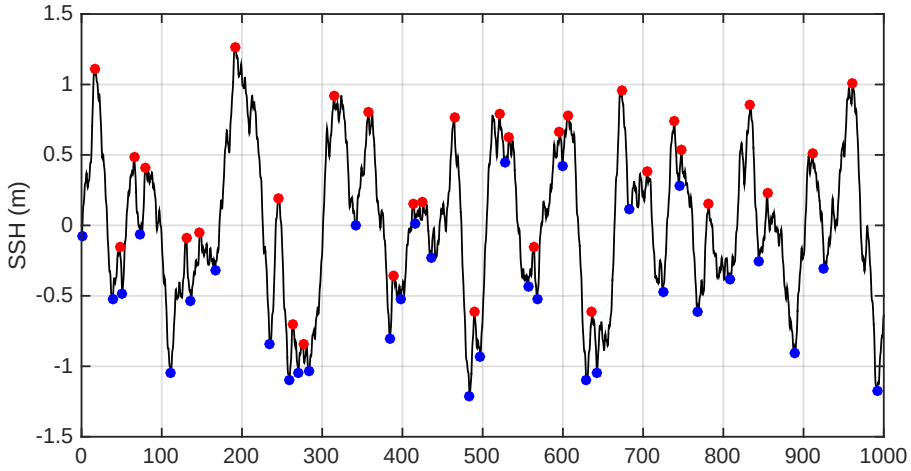

Figure S10: A sample sea surface height $\eta(x)$ calculated using the Bretschneider wave spectrum shown in Fig. S9. Shown is the first 1000 m of the wave record. Circles indicate local extrema which are used for calculating strain and subsequent floe sizes.

where $\Delta x_i^* \equiv x_i^* - x_{i-1}^*$. When the magnitude of this strain exceeds the critical strain, $\epsilon_{\text{crit}} = 3 \times 10^{-5}$, the floe will break. This determines a set of points at which a floe of thickness h will fracture, $X_i^*(h)$. From this set of points we define the size of the fractured floe as $X_{i+1}^* - X_i^*$. We form a histogram $R(r, h)$ of the number of occurrences of each fracture of size r, which is normalized so that $\int rR(r, h_s)\, dr = D$. In this way, $R(r, h_s)dr$ is equal to the number of fractures with size between r and $r+dr$ and thickness h_s when waves affect a fully ice-covered domain of length D. Figure S11 shows $R(1\text{m}, r)$ for realizations of the sea surface using the Bretschneider spectrum seen in Fig. S9. The histogram is calculated on a uniform grid in r of 1.3m resolution and then smoothed and interpolated to the high resolution of the FSTD model.

We assume that a floe of size s will fracture only when $X_{i+1}^* - X_i^* = r < s$, and that the number of fractures of size r is either proportional to $R(r)$ (for $r < s$), or zero (for $r >= s$). The total length of fractures of size r is thus proportional to $rR(r)$, or zero, for $r > s$. The floe size distribution formed by the fracture of a floe of size s, $F(\mathbf{s}, \mathbf{r})$ is therefore equal to the total length of floes of size r that are formed by this fracturing of a floe of size s, normalized

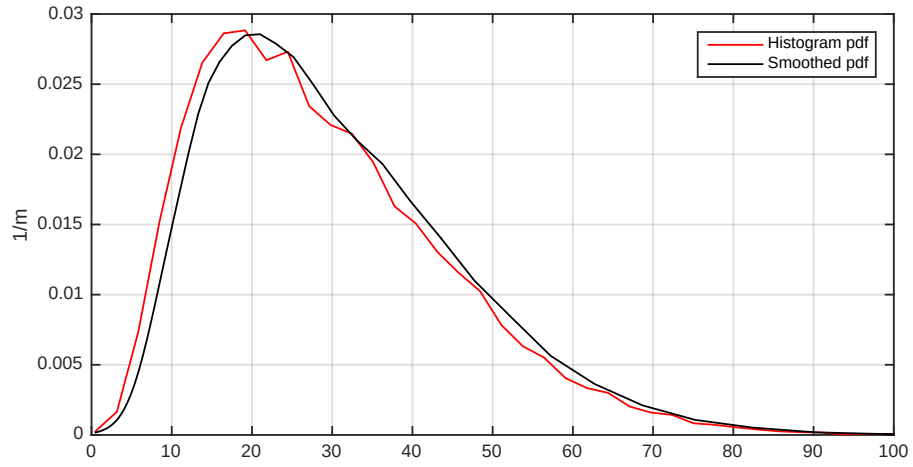

Figure S11: (red line) The probability (divided by the bin width) of a floe fracturing into each size class, calculated after 200 realizations of the sea surface height, with a uniform spatial discretization of 1.3m. (Black line) The same pdf smoothed and interpolated to the grid used in the FSTD model.

such that $\int_0^\infty F(\mathbf{s},\mathbf{r})d\mathbf{r} = 1$, i.e.,

$$F(\mathbf{s},\mathbf{r}) = F([s,h_s],[r,h]) = \frac{rR(r,h_s)}{\int_0^s rR(r,h_s)dr}\delta(h-h_s). \tag{3}$$

The upper limit of the normalization integral in the denominator is truncated to s because the integrand vanishes for larger values of r as explained above. The delta function $\delta(h-h_s)$ represents the fact that fracture does not change ice thickness, i.e., any floes formed from the fracture of ice with thickness h_s will also have thickness h_s.

The function $\Omega(\mathbf{r},t)d\mathbf{r}$ is the fractional area that belongs to floes of size between $\mathbf{r}$ and $\mathbf{r}+d\mathbf{r}$ that is fractured per unit time. It is set equal to the the area fraction covered by floes of size $\mathbf{r}$, f($\mathbf{r}$), multiplied by the fraction of the domain reached by waves of group velocity c_g per unit time, c_g/D, multiplied by the probability that floes of size $\mathbf{r}$ will fracture by waves. To calculate this probability, we note that $r'R(r')$ is the total length of the domain covered by waves that can break floes into size r'. Integrating this

over r' from zero to a size r we find the total width of the domain covered by waves that can produce floes smaller than r, which is the same as the length of the domain covered with waves that can break floes of size r into smaller sizes. Normalizing by the domain width D, we find the final factor in the expression for Ω,

$$\Omega([r,h],t) = f(\mathbf{r})\ (c_g/D)\left(\int_0^r r'R(r',h)dr'/D\right). \tag{4}$$

The group velocity is taken to be that of the mean zero-crossing wavelength, $c_g = \sqrt{\frac{\lambda_z g}{8\pi}}$. For the spectrum shown in Fig. S9, $c_g \approx 4.5$m/s. For the same spectrum, a sample calculated floe size distribution formed from the fracture of a floe of size $r = 100$m and thickness $h = 1m$, $F([r, 1\text{m}], [100\text{m}, 1\text{m}])$, is shown as Fig. S12. The third factor in Eq.4 is plotted as Fig. S12b for the same realizations.

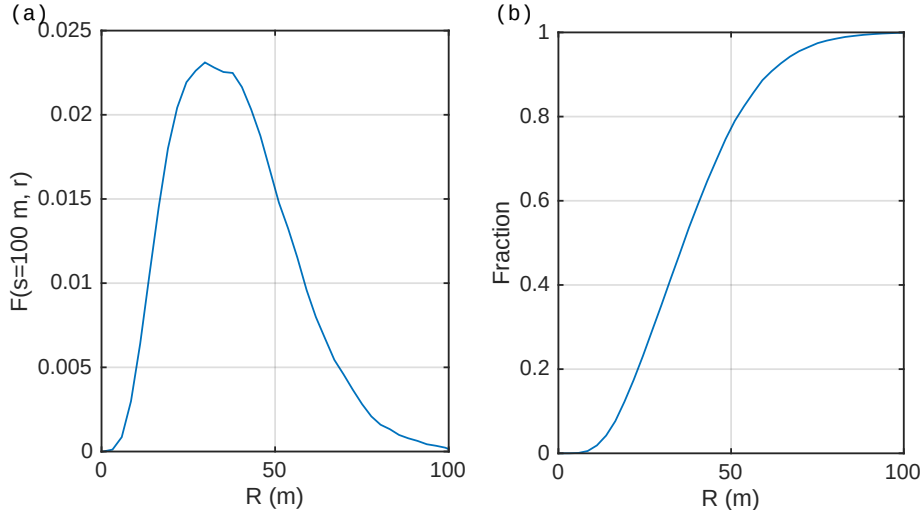

Figure S12: (a) The floe size distribution $F([100\text{m}, 1\text{m}], [r, 1\text{m}])$ formed by fracturing a floe of size 100 m and thickness 1 m by the wave spectrum shown in Fig. S9. (b) The third factor in eq. 4, for the same wave spectrum and a domain width of 10 km.

References

Bennetts, L. G. and Squire, V. a. (2012). Model sensitivity analysis of scattering-induced attenuation of ice-coupled waves. *Ocean Modelling*, 45-46:1–13.

Kohout, A. L. and Meylan, M. H. (2008). An elastic plate model for wave attenuation and ice floe breaking in the marginal ice zone. *J. Geophys. Res.*, 113(9):C09016.